Soil Dynamics and Earthquake Engineering 66 (2014) 13–30

Contents lists available at ScienceDirect

Soil Dynamics and Earthquake Engineering

journal homepage: www.elsevier.com/locate/soildyn

# Seismic performance of circular RC bridge columns with flexure–torsion interaction

Piguang Wang [a,b], Qiang Han [a,b,*], Xiuli Du [a,b]

[a] Key Laboratory of Urban Security and Disaster Engineering of Ministry of Education, Beijing University of Technology, Beijing 100124, China
[b] Beijing Collaborative Innovation Center for Metropolitan Transportation, Beijing 100124, China

ARTICLE INFO

*Article history:*
Received 25 April 2013
Received in revised form
14 April 2014
Accepted 28 June 2014
Available online 25 July 2014

*Keywords:*
RC column
Flexure–torsion interaction
Seismic performance
Hysteretic model

ABSTRACT

Reinforced concrete (RC) bridge columns for skewed, curved bridges and other kinds of irregular bridges can be subjected to combined loadings with axial load, shear force, flexure and torsion under multi-dimensional earthquake excitations. Combined loadings including torsion probably affect the seismic performance of these bridge columns. The experimental investigation on the seismic performance of circular RC bridge columns under combined cyclic bending and torsional loading is conducted in this paper. Twelve circular RC bridge column specimens are tested under various loading conditions: cyclic bending, cyclic torsion, and combined cyclic torsion and cyclic bending. Several combinations of cyclic bending and cyclic torsion are applied to evaluate the interaction between torsion and flexural capacity of bridge columns. The experimental results showed that the flexural capacity decreases and the damage tends to occur upward outside the flexural plastic hinge region as the level of applied cyclic torsion increases, and the torsional capacity decreases as the level of applied cyclic bending increases. The failure mode and deformation characteristics of RC bridge columns will be changed due to the effect of combined flexural and torsional loadings. The locking and unlocking effect of the spiral reinforcement on torsional and flexural envelopes of columns under pure torsion and combined cyclic bending and torsion is found. The influence of aspect ratio, longitudinal reinforcement ratio and type of spiral reinforcement on the seismic performance of columns under combined action with the same rotation-drift ratio is also discussed. An empirical flexural and torsional hysteretic model for circular RC columns with single spiral stirrup under combined cyclic bending and torsion is proposed based on the experimental results.



## 1. Introduction

Curved bridges, skewed bridges and other kinds of bridges with special configurations are widely used because of the space limitation for the transportation system in many urban and mountainous areas in China. Those bridges are more susceptible to suffer earthquake damage because of structural asymmetry, soil conditions, movement of joints, abutment restraints, and rigid decking. Particularly, reinforced concrete (RC) bridge columns of the irregular bridge structures could be subjected to the combination of axial force, shear force, flexural moments, and torsional moments under multi-directional ground motions, which can result in complex flexural and shear failure of these bridge columns. Many RC bridge columns of curved and skewed bridges suffered severe damages or even collapsed during the 2008 Wenchuan earthquake in China [1], as shown in Fig. 1. Therefore, it is necessary to investigate the seismic performance of RC bridge columns under combined torsional moment, bending moment and axial loading.

In the past few decades, extensive experimental and analytical studies have been carried out by Priestly et al. [2,3], Lehman et al. [4], Wehbe et al. [5], Yeh et al. [6] Pinto et al. [7] and Phan et al. [8] to investigate the seismic performance of rectangular/circular columns subjected to the combination of axial force and cyclic flexural loading. The various hysteretic models to predict responses of RC columns under axial force and bending load or bending and shear force are proposed by Clough and Johnston [9], Takeda et al. [10], Park and Ang [11], Ozcebe and Saatcioglu [12], and Kowalsky and Priestley [13]. When bridges are subjected to multi-directional earthquake excitations, most of the bridge columns will undergo the combination of axial force, shear force, bending and torsion, especially for those bridge piers of skewed, curved bridges and other kinds of irregular bridges. The behavior of RC bridge columns under combined axial force, bending and torsion is different from the case with axial force plus uniaxial bending. However, there is a lack of information on RC bridge columns subject to combined action of axial force, bending and

* Corresponding author at: Beijing University of Technology, Beijing 100124, China. Tel.: +86 10 67292500.
*E-mail address:* qhan@live.com (Q. Han).

http://dx.doi.org/10.1016/j.soildyn.2014.06.028
0267-7261/

**Fig. 1.** Column damage of Huilan interchangebridge (2008 Wenchuan earthquke, China).

torsion in seismic regions. Few studies on the seismic performance, failure criterion and analytical model of solid RC circle/square columns under combined bending and torsion loadings have been investigated by Otsuka et al. [14,15], Tirasit and Kawashima [16,17], Belarbi et al. [18,19,20], Prakash et al. [21], Li et al. [22], Mullapudi and Ayoub [23,24], and Li and Belarbi [25]. The seismic performance of bridge columns is determined based on the unilateral cyclic loading test and bridge columns are designed independently in longitudinal and transverse directions, and the bridge RC columns for these irregular bridges have not carefully considered the effect of torsional moments in current Chinese bridge seismic design code [26]. The complicated behavior of RC bridge columns under multi-dimensional earthquake excitation is not well understood and there is no efficient hysteretic model available. So the improved analytical models are needed for simulating the hysteretic behavior of RC bridge columns for curved and skewed bridges subjected to multi-directional earthquake excitation components.

The main objectives of this paper are: (1) to evaluate seismic performance, failure modes and deformation characteristics of RC circular bridge columns subject to combined flexural and torsional loadings; (2) to compare the seismic performance of such columns under bending and torsion interaction with those subjected to uniaxial bending or torsion; (3) to present a hysteretic model to predict the response of circular RC columns under combined flexural and torsional loadings.

## 2. Experimental program

### 2.1. Specimen details and material properties

Twelve specimens were designed to be representative of typical RC circular bridge columns existing Chinese bridge engineering practice. The dimension and reinforcement layout of the twelve specimens are shown in Fig. 2. Table 1 shows specimen properties and test cases of the twelve columns. Each of the circular RC columns had a diameter of 400 mm and a clear cover of 25 mm. The total height of the column was 2350 mm and the effective height measured from the bottom of the column to the loading point was 1600 mm. Twelve RC column specimens were tested under a constant axial load $0.1f'_cA_g$ or $0.2f'_cA_g$, which were the estimated weights of the bridge deck. $f'_c$ is the concrete compressive strength, and $A_g$ is the gross section area. In Table 1, there are three forms of stirrup including circular stirrup, single spiral stirrup and cross spiral stirrup. The single spiral stirrup denotes a single spiral bar wrapped around longitudinal bars spaced near the perimeter of the member. The cross spiral stirrup is made by using two spiral bars wrapped around longitudinal bars. And the directions of spiral

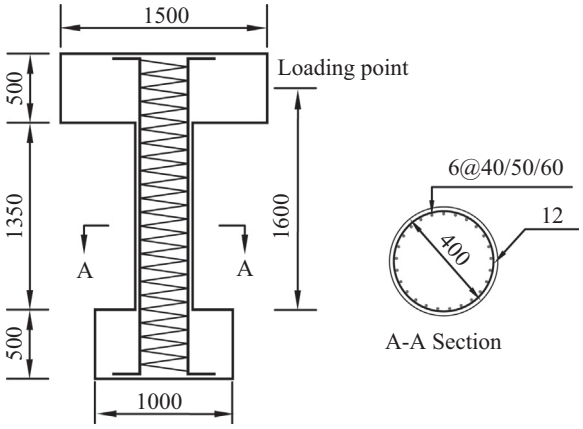


**Fig. 2.** Specimen configuration and reinforcement (Unit: mm).

**Table 1**
Specimen properties and test cases.

| Column | $r$ | Axial load ratio | Axial compression (kN) | Longitudinal ratio | Stirrup spacing (mm) |
|---|---|---|---|---|---|
| S1 | 0 | 0.1 | 230 | 0.015 | 50 |
| S2 | ∞ | 0.1 | 230 | 0.015 | 50 |
| S3 | 0.5 | 0.1 | 230 | 0.015 | 50 |
| S4 | 2 | 0.1 | 230 | 0.015 | 50 |
| S5 | 4 | 0.1 | 230 | 0.015 | 50 |
| S6 | 1 | 0.2 | 460 | 0.015 | 50 |
| S7 | 1 | 0.2 | 460 | 0.022 | 50 |
| S8 | 1 | 0.2 | 460 | 0.011 | 50 |
| S9 | 1 | 0.2 | 460 | 0.015 | 40 |
| S10 | 1 | 0.2 | 460 | 0.015 | 60 |
| S11 | 4 | 0.1 | 230 | 0.015 | 50 (circular stirrup) |
| S12 | 4 | 0.1 | 230 | 0.015 | 50 (cross spiral) |

of the two spiral bars are opposite. In addition, the circular stirrup is made by welding a bar into a ring. Same conventional steel and concrete materials were used in the prototype and model bridge columns, resulting in a scaling factor of 1.0 for stresses. The longitudinal reinforcing bars were 12 mm in diameter with design yield strength $f_y = 335$ MPa. The spiral reinforcing bars were 6 mm in diameter with a design yield strength$f_y = 235$ MPa. The concrete had design compressive strength$f_c' = 19.1$ MPa at 28 days. The design yield strength for bars ($f_y$) means the characteristic yield strength divided by partial material safety factor and the design compressive strength for concrete ($f_c$) means he characteristic compressive strength divided by partial material safety factor. The average measured values of the yielding strength; ultimate stress and ultimate strain of reinforcing steel coupons from standard tensile tests were 392 MPa, 498 MPa and 16%, respectively. The actual average compressive strength of concrete was $f_{cu}' =$ 42.6 MPa, which was determined by $150 \times 150 \times 150$ mm$^3$ concrete testing after 28-day curing process. Both the actual reinforcing steel and concrete strengths were higher than the expected design strengths.

### 2.2. Test setup

The test program was conducted in the Key Laboratory of Urban Security and Disaster Engineering of Ministry of Education of P.R. China at Beijing University of Technology, China. Fig. 3 shows the photos of the specimens and loading scheme. The specimen was mounted vertically on strong floor and the top end of the column was held by a hydraulic jack that provided a constant axial load. The tests were conducted under lateral displacement and rotation control. Cyclic uniaxial bending, torsion, and combined bending and torsion were generated by controlling two horizontal actuators as shown in Fig. 4. Cyclic uniaxial bending was created by applying equal displacement commands in the two actuators. Pure torsion was created by applying equal but opposite displacement commands in the two actuators. Combined cyclic torsion and uniaxial bending were imposed by applying different displacement command in the two actuators.

### 2.3. Loading protocol

It is common to use force control, displacement control and force–displacement hybrid control for uniaxial quasi-static tests. In order to control the level of combined bending and torsion, a non-dimensional parameter called "rotation-drift ration" [17], r is introduced here to define the level of combined cyclic bending

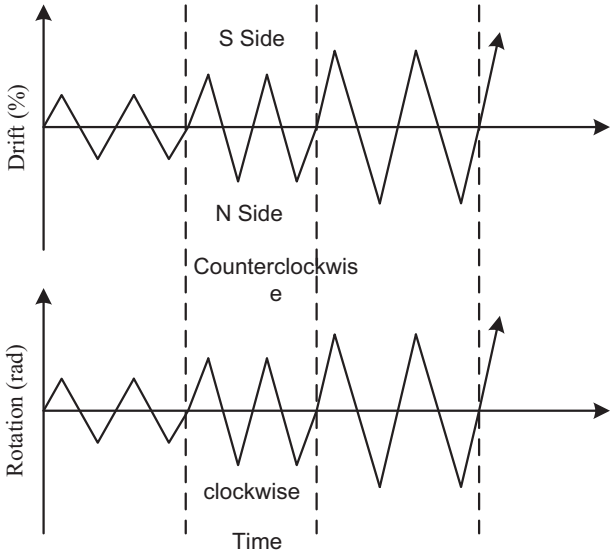


**Fig. 5.** Loading protocol.

**Fig. 3.** Specimens and loading scheme.

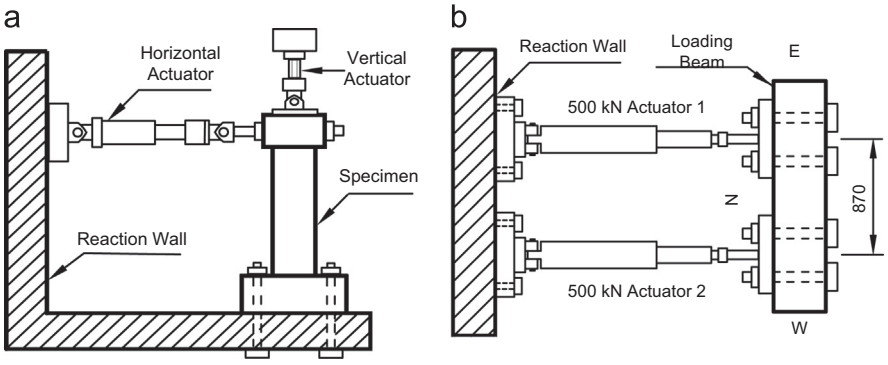


**Fig. 4.** Test setup; (a) side view, and (b) top view.

and torsion as

$$r = \frac{\theta}{\Delta} \tag{1}$$

$$\Delta = \frac{\delta}{L_{eff}} \tag{2}$$

where $\theta$ is the column rotation (radian), $\Delta$ is the lateral drift of column, $\delta$ is the lateral displacement at effective height $L_{eff}$ which is measured from the bottom to the loading point.

The rotation-drift ratios r and applied lateral drifts and rotations of each loading step of bridge columns are presented in Fig.5 and Table 2. S1 was tested under cyclic uniaxial bending and S2 was tested under pure cyclic torsion. S3, S6, S4 and S5 were loaded with varying the rotation-drift ratio $r$ as 0.5, 1, 2, and 4, respectively. The lateral drift and rotation were simultaneously applied two cycles at every loading step. S7 to S10 were loaded with the same lateral drifts and rotations as S6 at each loading step, while S11 and S12 were loaded with the same lateral drifts and rotations as S5.

Based on the above parameters, we can get the shear strength of the columns by ACI code [27], which is about 185 kN including the shear strength provided by concrete and stirrup with 98 kN and 87 kN, respectively. It can be seen that shear strength is greater than the applied load which is less than 120 kN. That is to say, shear–flexure interaction can be eliminated from the discussion on test observations.

**Table 2**
Applied lateral drifts and rotations of each loading step.

| Step | | 1 | 2 | 3 | 4 | 5 | 6 | 7 | 8 | 9 | … |
|---|---|---|---|---|---|---|---|---|---|---|---|
| S1 | drift (%) | 0.25 | 0.5 | 1 | 1.5 | 2 | 2.5 | 3 | 3.5 | 4 | … |
| S2 | $\theta$ (rad) $\times 10^{-2}$ | 0.25 | 0.5 | 1 | 2 | 3 | 4 | 5 | 6 | 7 | … |
| S3 | $\theta$ (rad) $\times 10^{-2}$ | 0.125 | 0.25 | 0.5 | 0.75 | 1 | 1.25 | 1.5 | 1.75 | 2 | … |
| | drift (%) | 0.25 | 0.5 | 1 | 1.5 | 2 | 2.5 | 3 | 3.5 | 4 | … |
| S4 | $\theta$ (rad) $\times 10^{-2}$ | 0.25 | 0.5 | 1 | 1.5 | 2 | 2.5 | 3 | 3.5 | 4 | … |
| | drift (%) | 0.125 | 0.25 | 0.5 | 0.75 | 1 | 1.25 | 1.5 | 1.75 | 2 | … |
| S5 | $\theta$ (rad) $\times 10^{-2}$ | 0.25 | 0.5 | 1 | 1.5 | 2 | 2.5 | 3 | 3.5 | 4 | … |
| | drift (%) | 0.0625 | 0.125 | 0.25 | 0.375 | 0.5 | 0.625 | 0.75 | 0.875 | 1 | … |
| S6 | $\theta$ (rad) $\times 10^{-2}$ | 0.25 | 0.5 | 1 | 1.5 | 2 | 2.5 | 3 | 3.5 | 4 | … |
| | drift (%) | 0.25 | 0.5 | 1 | 1.5 | 2 | 2.5 | 3 | 3.5 | 4 | … |

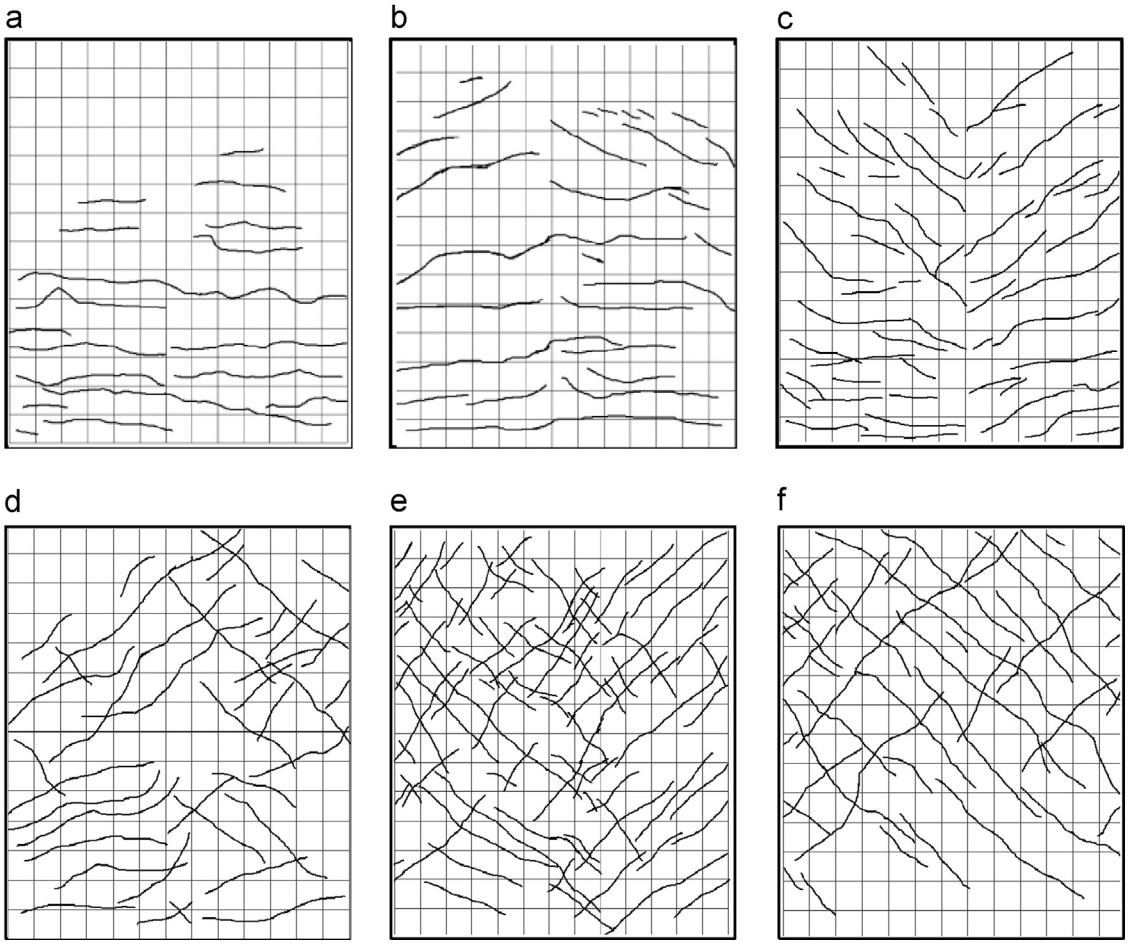


**Fig. 6.** The cracks distribution of the specimens under different levels of combined cyclic bending-torsional interaction; (a) S1 $r$=0, (b) S3 $r$=0.5, (c) S5 $r$=1, (d) S2 $r$=2, (e) S5 $r$=4, and (f) S2 $r$=$\infty$.

## 3. General observations

Fig. 6 shows crack in the bending load condition for column S1, torsion load condition for column S2, and bending and torsion loads condition for column S3, S6, S4 and S5, respectively. Fig. 7 shows the damage region of columns under different levels of combined bending and torsion.

The column S1 tested under pure flexure load initially exhibited horizontal flexural cracks in the range of 100–500 mm (100, 200, 350, 500 mm) from the bottom of the column on side S and N at a drift of about 0.5%. These cracks continued to grow and new cracks appeared on both sides of the column with drift increasing. The cover concrete crushing began to take place with compression failure in the plastic hinge region on side S at drift 2.5% and the cover concrete started to spall at drift 3%. Before failure, tension occurs in a large portion of the section in the plastic hinge region, causing the tension steel bars to yield before actual crushing of the concrete. Subsequently, the column failure began with a flexural plastic hinge with 200 mm height from the base of the column, followed by core concrete degradation, and finally by the buckling of longitudinal bars on the compression side. At failure, the strain in the tension steel is greater than the yield strain. It can be seen from Fig. 6(a) that all cracks under pure bending for column S1 were horizontal circular cracks.

The column S2 tested under pure torsion initially exhibited diagonal cracks at 0.005 radian rotation. Subsequently, the number of diagonal cracks increased and the checker board cracks developed on all column sides, while the width of those cracks expanded with the applied rotation increasing. It should be noted that significant diagonal cracks started developing near mid-height on the column. The cover concrete started to spall outward at 0.05 radian rotations. Then, the significant damage took place at the mid-height column. It is the typical characteristic in the pure torsional failure for a plain RC member that it cracks and fails along 45° spiral lines due to the diagonal tension corresponding to the torsional stresses. Fig. 6(f) shows that all cracks of column S2 were diagonal the angles of cracks relative to the column cross section were about 45°. Fig. 7(e) shows that the column S2 damaged with a torsional plastic with 500 mm height near the mid-height of the column, which was between the bottom 500 mm and 100 mm from the base of the column. The damage pattern of the column under pure torsion was significantly different from that of S1 under cyclic bending.

The progress of damage of S3 ($r=0.5$) was very similar to S1 which was subjected to cyclic bending. Cracks first occurred at 0.00125 rad – 0.25% drift near the bottom 350 mm and 500 mm from the base of the column on side S, and then cracks developed on all sides. However, those cracks did not form horizontally as S1. In comparison with S2, the angles of cracks relative to the column section were much smaller in S3, and the checker board cracks did not occur because the increase of the longitudinal compressive stress from the bending moment reduced the diagonal tensile stress from torsion. On the other hand, the damage zone of S3 was larger than S1.

The progress of damage of S6 ($r=1$) was also very similar to S1. Diagonal cracks first occurred at 0.0025 rad – 0.25% drift in the range of 100–500 mm from the base mainly on side S and N in S6 ($r=1$). Subsequently, the number of diagonal cracks increased, and the checker board cracks did not occur. However, the angles of those cracks were much larger than in S3.

On the other hand, diagonal cracks first occurred at 0.0025 rad – 0.125% drift in S4 ($r=2$). The angles of cracks were larger than those of the former columns with smaller $r$ and the checker board cracks developed on all surfaces, but the extent of checker board cracks was a little sparser than S2. This implied that the effect of torsion became predominant. The progress of damage of S5 ($r=4$) was also very similar to S2. The angles of cracks and the extent of checker board cracks were very similar to S2, which implied that the effect of torsion became predominant. But the failure position

**Table 3**
Angles of cracks of columns under different levels of combined cyclic bending–torsional action.

| $r$ | 0 | 0.5 | 2 | 4 | ∞ |
|---|---|---|---|---|---|
| The bending zone (deg) | 0 | 0 | 20 | 30 | 45 |
| The other zone (deg) | 0 | 25 | 40 | 45 | 45 |

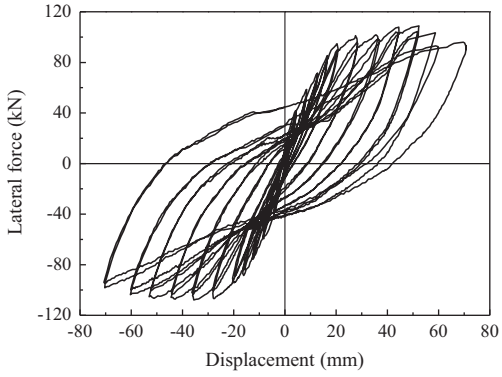


**Fig. 8.** Hysteresis loop of column S1.

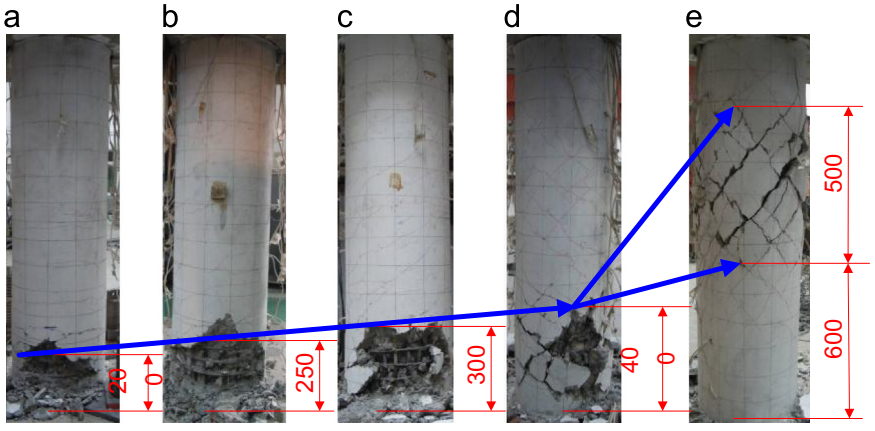


**Fig. 7.** Failure region of the specimens under different levels of combined cyclic bending–torsional interaction; (a) S1 $r=0$, (b) S3 $r=0.5$, (c) S5 $r=2$, (d) S5 $r=4$, and (e) S2 $r=\infty$.

was mainly on the base of the column with 400 mm height while the failure position of S2 was near the mid-height of the column.

It can be seen from Fig. 6 that the angles of cracks were likely to expand as $r$ increased. Table 3 shows the angles of cracks under different levels of combined bending and torsion. On the other hand, Fig. 7 shows that the extent of the damage region was likely to expand as r increased. The lengths of damage zones were about 200 mm in S1 ($r=0$), 250 mm in S3 ($r=0.5$), 300 mm in S4 ($r=2$), 400 mm in S5 ($r=4$), and 500 mm in S2 ($r=\infty$).

Based on the above and research work by Mosley et al. [28], we can draw that diagonal cracks will usually develop from the top of flexural cracks when a bending moment is present. And the flexural cracks themselves slightly reduce the torsional stiffness provided that the diagonal cracks do not develop. The final mode of failure will depend on the magnitude of rotation-drift ration, the distribution and quantity of reinforcement present.

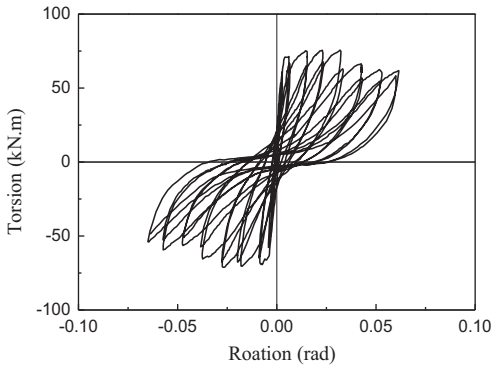


**Fig. 9.** Hysteresis loop of column S2.

## 4. Experimental results and analysis

### 4.1. Hysteretic behavior of columns

The flexural hysteresis of column under pure bending (S1) is shown in Fig. 8. The restoring force was stable between 1.25% and 3.75% drift with a flexural strength corresponding to a lateral load of 107.9 kN at 2.5% drift. Subsequently, the flexural restoring force started to deteriorate as a result of the compression failure of cover concrete and the buckling of longitudinal bars, and the column lost the lateral confinement and its restoring force reached 85% of its maximum strength. This is the typical progress of the damage in the flexural failure of cantilever column.

The torsional hysteresis of column under pure torsion (S2) is shown in Fig. 9. It can be seen that the torsional stiffness deteriorated sharply after cracking at 0.005 radian rotation. That is to say, the torsional hysteresis is approximately linear up to cracking and after that it becomes nonlinear with a drop in the torsional stiffness. During the positive cycles of loading, the torsional strength reached 75 kN · m at 0.03 radian followed by a sharp deterioration, and during the negative cycles of loading, the torsional strength reached 70 kN · m at 0.02 radian followed by a sharp deterioration. It can be seen that the torsional strength and ductility levels are different in the positive and negative loading cycles, which is caused by the locking and unlocking effect of the spirals. This phenomenon was also found by Belarbi et al. [20]. In this paper, locking represents that the spiral stirrup twists along

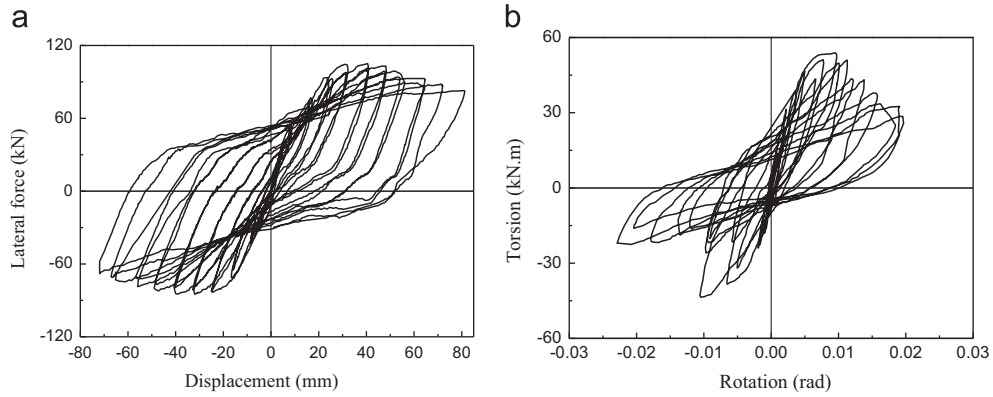


**Fig. 10.** Hysteresis loops of column S3 ($r=0.5$); (a) flexural hysteresis loop, and (b) torsional hysteresis loop.

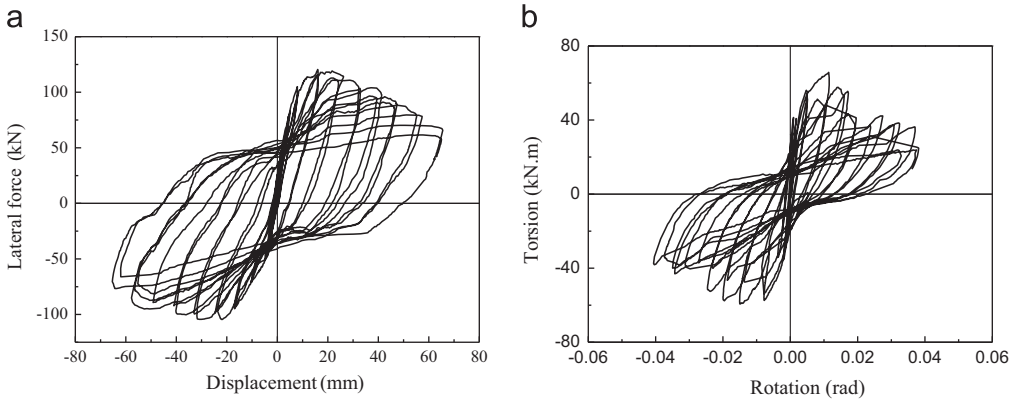


**Fig. 11.** Hysteresis loops of column S6 ($r=1$); (a) flexural hysteresis curves, and (b) torsional hysteresis curves.

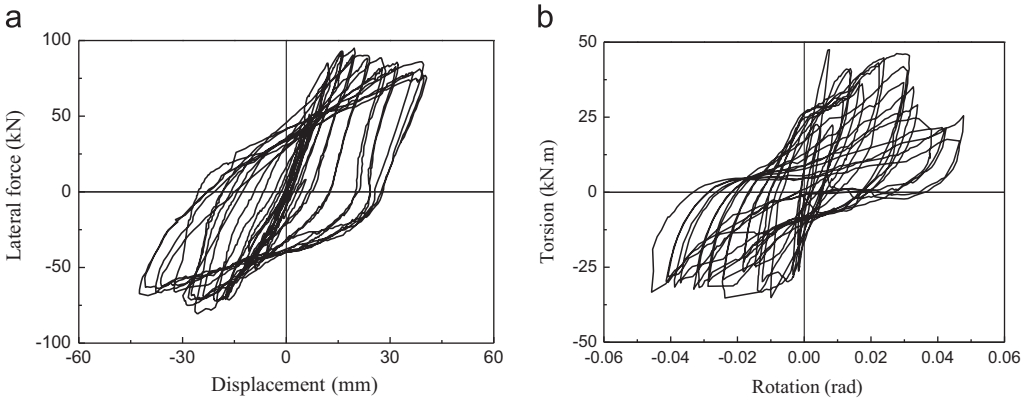


**Fig. 12.** Hysteresisloops of column S4 ($r=2$); (a) flexural hysteresis curves, and (b) torsional hysteresis curves.

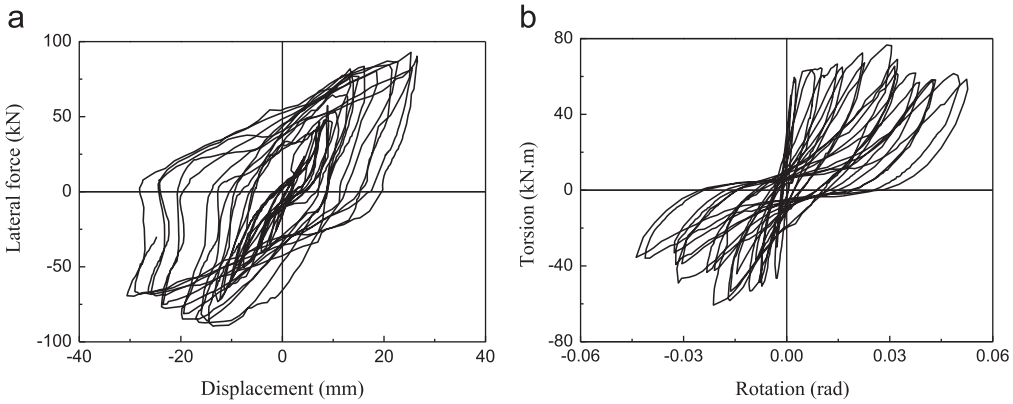


**Fig. 13.** Hysteresis loops of column S5 ($r=4$); (a) flexural hysteresis curves, and (b) torsional hysteresis curves.

the direction of spiral, while unlocking represents that the spiral stirrup twists along opposite direction of spiral. During the positive cycles of twisting, the spirals were unlocked which helped to cause significant spalling and reduced the confinement effect on the concrete core. On the other hand, during the negative cycles of loading, the spirals were locked and contributed more to the confinement of the concrete core. This effect is reflected in the asymmetrical nature of the observed hysteresis loop at higher levels of loading. At higher ductility levels, the load resistance on the negative cycles was higher than that under positive cycles of loading due to the added confinement generated by the locking effect of the spirals.

Figs.10–13 show the flexural hysteresis and torsional hysteresis of S3–S6 under combined bending and torsion with different $r$. It can be clearly seen that the flexural and torsional hysteresis under moderate to large $r$ were quite different from the hysteresis under pure cyclic bending and pure cyclic torsion. The flexural strength column decreased while the torsional strength increased as $r$ increased besides S6 ($r=1$). The flexural strength and the torsional strength of S6 ($r=1$) was a little greater than that of S3 ($r=0.5$), which resulted from the effect of larger axial compressive force. On the other hand, the flexural restoring force and torsional strength are different in the positive and negative loading cycles, which are caused by the locking and unlocking effect of the spirals.

### 4.2. The effects of different factors under the same r

Figs. 14–17 compare the envelopes of flexural and torsional hysteresis of columns with different $r$, different reinforcement ratio, different stirrup spacing and different type of stirrups.

Fig. 14 shows that the deterioration of flexural strength and ductility capacity occurred as $r$ increased, which is mainly due to the effect of torsion. It is noted that a stable lateral force zone in which the lateral restoring force was nearly constant between 1.25% and 3.75% drift in the flexural hysteresis ($r=0$) became less significant as $r$ increased. Likewise, the deterioration of torsional strength and ductility capacity occurred as $r$ decreased, and the hysteretic envelope under combined action became close to that under pure cyclic torsion as $r$ increased. Besides, the asymmetrical nature of the torsional and flexural envelopes which was due to the locking and unlocking effect of the spirals was also significantly obvious.

Fig. 15 shows that the flexural strength of columns under combined bending and torsion with the same $r$ was improved as the reinforcement ratio increased, especially the flexural strength after the peak point of the same displacement was improved obviously. However, the torsional strength of columns under combined bending and torsion with the same $r$ was not influenced obviously by the reinforcement ratio.

Fig. 16 shows that the torsional strength of columns under combined bending and torsion with the same $r$ was improved as the stirrup spacing decreased; especially the torsional strength of the positive loading cycles (unlocking orientation of the spirals) was improved obviously. But the influence of the stirrup spacing to the flexural of columns under combined bending and torsion with the same $r$ was not obvious.

Fig. 17 shows that the flexural strength and torsional strength of positive loading cycles under combined bending and torsion with the same $r$ was larger than that of negative loading cycles for the single spiral columns, which was caused by the locking and unlocking effect. However, the flexural strength and torsional

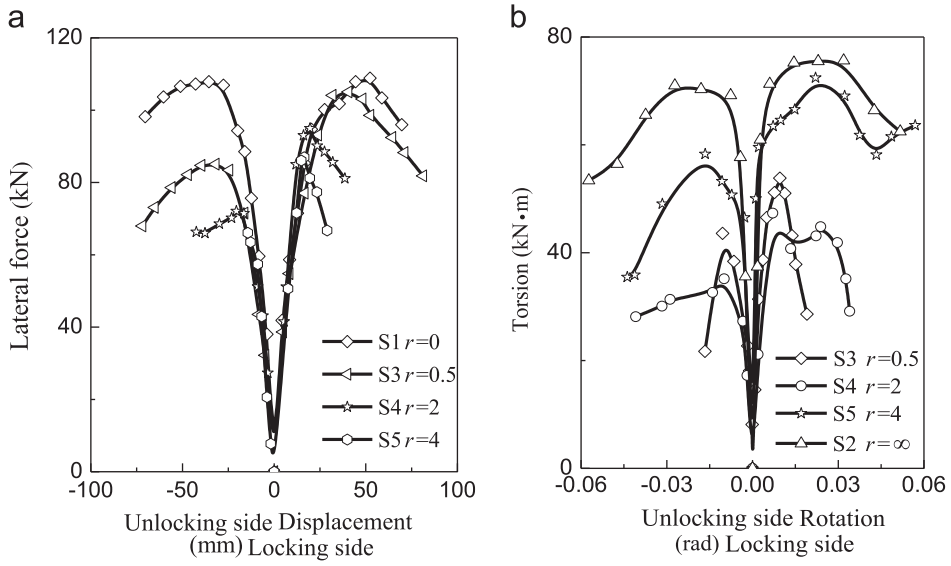


**Fig.14.** Hysteretic envelopes on combined cyclic bending and torsion with different *r*; (a) flexural hysteretic envelopes, and (b) torsional hysteretic envelopes.

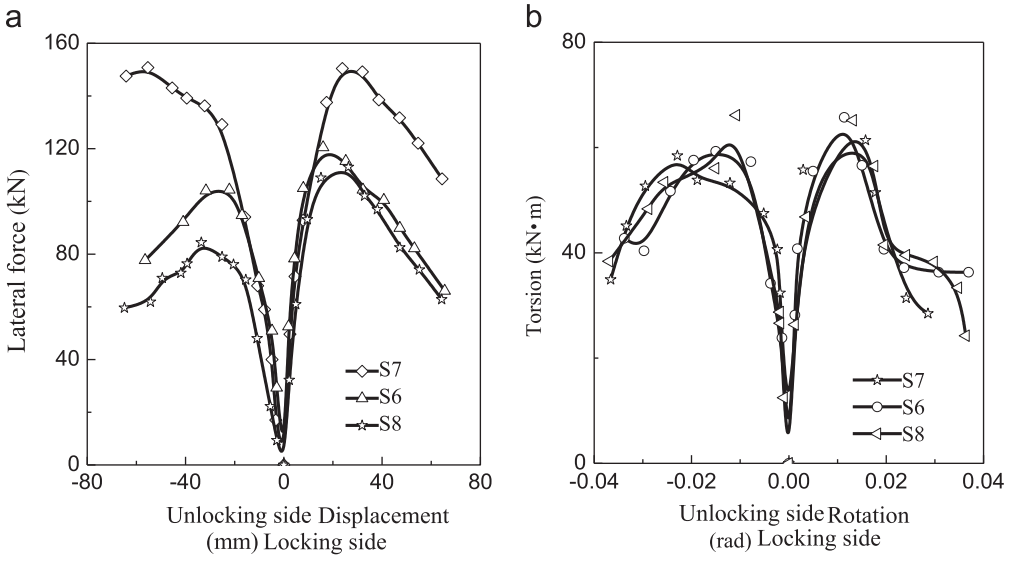


**Fig. 15.** Hysteretic envelopes of combined cyclic bending and torsion with different reinforcement; (a) flexural hysteretic envelopes, and (b) torsional hysteretic envelopes.

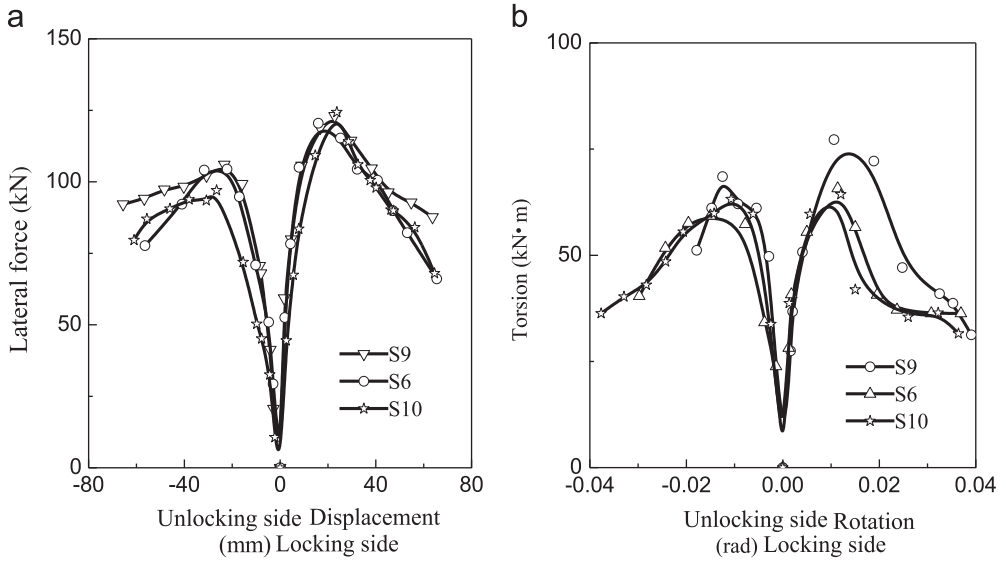


**Fig. 16.** Hysteretic envelopes of combined cyclic bending and torsion with different stirrup spacing; (a) flexural hysteretic envelopes, and (b) torsional hysteretic envelopes.

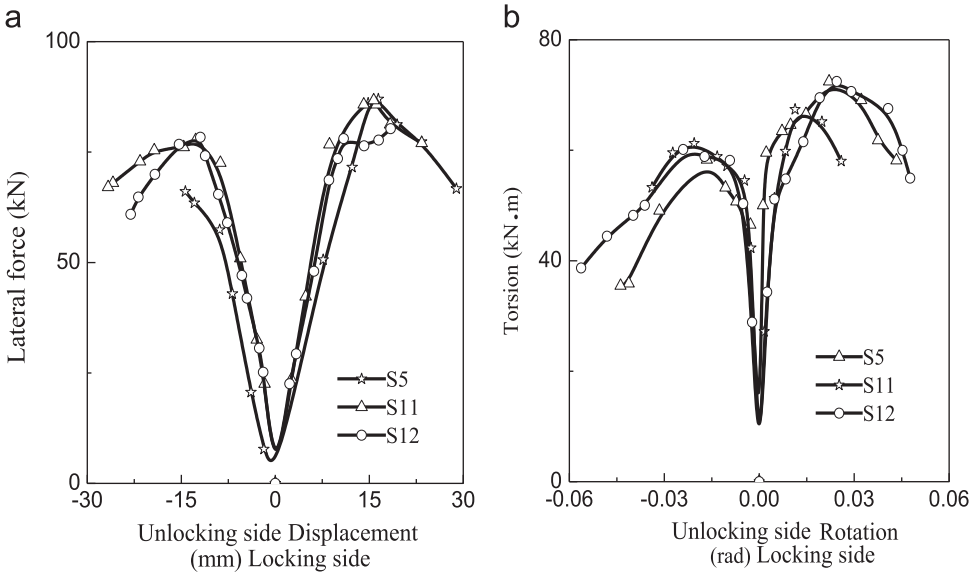


**Fig. 17.** Hysteretic envelopes of combined cyclic bending and torsion with different type of stirrups; (a) flexural hysteretic envelopes, and (b) torsional hysteretic envelopes.

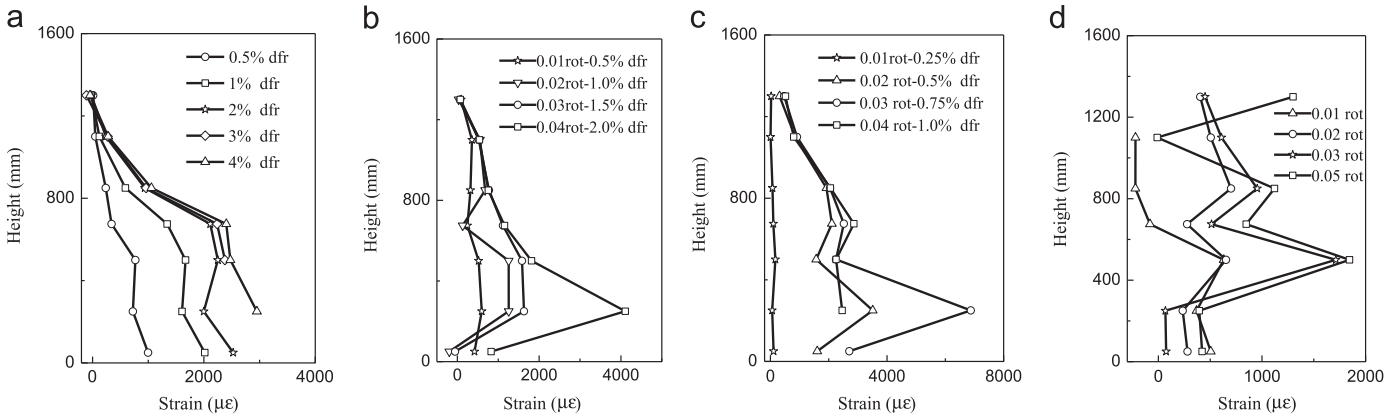


**Fig. 18.** Variation of maximum strains of the longitudinal reinforcements with the column height; (a) S1 $r=0$, (b) S4 $r=2$, (c) S5 $r=4$, and (d) S2 $r=\infty$.

strength of the cross spiral columns and circular stirrup columns were almost the same between the two directions. The idea of using two cross spirals to enhance the strength and ductility characteristics and eliminate the locking and unlocking effect was also studied by Hindi et al. [29]. Their results indicated that the cross spiral columns were more strength and ductile. Comparing single spiral and cross spiral columns with the same amount of confining steel, the cross spiral columns rotated significantly larger amount before yielding. Strength deterioration was greatly reduced by cross spiral confinement. The cross spirals tended to reach maximum capacity and continue to maintain a higher level of capacity through several large deformation cycles.

### 4.3. Strain of reinforcement

Fig. 18 shows the variation of maximum strains in the longitudinal reinforcements along the column height. Peak strains of the longitudinal reinforcements took place at 50 mm, 250 mm, 500 mm, 500 mm, 675 mm, 850 mm, and 1100 mm from the bottom of column in each specimen. It can be clearly seen that the locations of peak strains in the longitudinal reinforcement were shifted from the base to the middle of column as $r$ increased.

## 5. Flexural hysteretic model

The proposed flexural hysteresis consists of two parts. The first part is the primary force–displacement relationship under monotonic loading. After obtaining the empirical primary curves of the hysteresis, the unloading and reloading criteria are required to capture the hysteretic behavior, which is the second part. Presently, there have been kinds of hysteretic models for flexure RC members [9,10,12]. These models are capable to idealize many phases of loading, unloading, and reloading branches of force–displacement relationships under cyclic bending load, but these models cannot be used to simulate the flexural hysteretic behavior of RC columns under combined cyclic bending and torsion loadings. The flexural hysteretic model is proposed considering the factors of rotation-drift ratio $r$ and the number of loading cycles according to the experimental data. The method that hysteretic model is proposed according to the experimental data was also used to determine hysteretic shear model of RC members by Ozcebe and Saatcioglu [12].

### 5.1. Primary curves

The proposed primary curve for the flexural hysteretic model is idealized as shown in Fig. 19. The column is assumed to be elastic

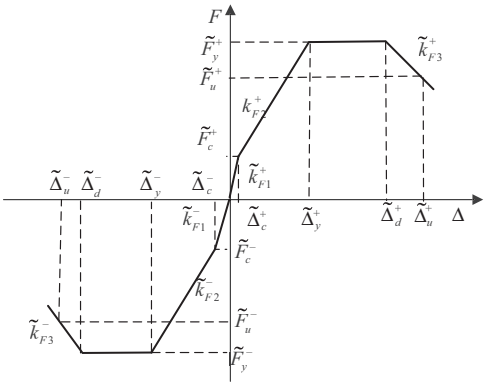


**Fig. 19.** Proposed primary curve for flexure.

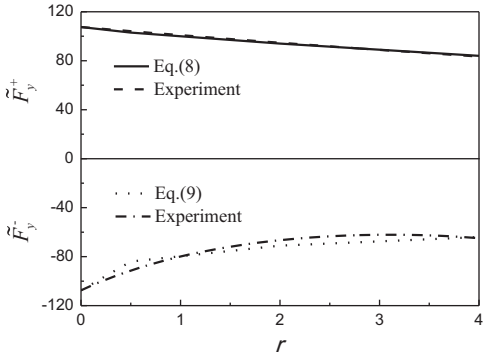


**Fig.20.** Dependence of the flexural strength $\tilde{F}_y$ on $r$.

with an initial flexural stiffness $\tilde{k}_{F1}$ until the lateral force reaches the flexural strength $\tilde{F}_c$ at the cracking drift $\tilde{\Delta}_c$. Afterwards, the column access to elastoplastic stage with a linear flexural stiffness $\tilde{k}_{F2}$ until the lateral force reaches the flexural strength $\tilde{F}_y$ at the yield drift $\tilde{\Delta}_y$. This lateral force remains constant until the column is loaded to $\tilde{\Delta}_d$, and then degrades with a negative flexural stiffness $\tilde{k}_{F3}$ to the ultimate lateral force $\tilde{F}_u$ which is equal to 80% of the flexural strength at $\tilde{\Delta}_u$. The flexural stiffness is defined as

$$\tilde{k}_{F1} = \frac{\tilde{F}_c}{\tilde{\Delta}_c L_{eff}} \tag{3}$$

$$\tilde{k}_{F2} = \frac{\tilde{F}_y - \tilde{F}_c}{(\tilde{\Delta}_y - \tilde{\Delta}_c) L_{eff}} \tag{4}$$

$$\tilde{k}_{F3} = \frac{\tilde{F}_u - \tilde{F}_y}{(\tilde{\Delta}_u - \tilde{\Delta}_y) L_{eff}} \tag{5}$$

where $L_{eff}$ denotes the effective height of column. It is noted that $L_{eff}$ is used here in order to produce the unit flexural stiffness in force per unit length.

It can be seen from the experimental results shown in the previous section that the behavior of the RC columns depended on the rotation-drift ratio $r$. Moreover, the flexural strength of positive loading is generally larger than that of negative loading. The dependency of the lateral restoring force and the displacement of the columns on the rotation-drift ratio $r$ is clarified based on the regression analysis. It is noted that the parameters of positive loading are represented with $X^+$, while the parameters of negative loading are represented with $X^-$.The lateral restoring force $\tilde{F}_c$ and $\tilde{F}_y$ of the column under combined action deteriorated as $r$ increased, and the relationships may be approximated as

$$\tilde{F}_c^+ = (e^{-0.178r}) F_c \tag{6}$$

$$\tilde{F}_c^- = (e^{-0.493\sqrt{r}}) F_c \tag{7}$$

$$\tilde{F}_y^+ = (e^{-0.0634r}) F_y \tag{8}$$

$$\tilde{F}_y^- = (e^{-0.283\sqrt{r}}) F_y \tag{9}$$

$$\tilde{F}_u = 0.8\tilde{F}_y \tag{10}$$

where $F_c$ is the cracking load and $F_y$ is the yield load of the column under cyclic bending, respectively. As shown in Fig. 20, Eqs. (8) and (9) give a good approximation with the experimental results.

Similarly, it can be found from Table 4 that the cracking drift $\tilde{\Delta}_c$, the yield drift $\tilde{\Delta}_y$, the drift when the lateral restoring force starts to deteriorate $\tilde{\Delta}_d$ and the ultimate drift $\tilde{\Delta}_u$ degrades with the increase of rotation-drift ratio $r$. The relationships can be described as the following forms

**Table 4**
Dependence of $\tilde{\Delta}_y$, $\tilde{\Delta}_d$and $\tilde{\Delta}_u$ on $r$.

| $r$ | 0 | 0.5 | 2 | 4 |
|---|---|---|---|---|
| Crack displacement (mm) | | | | |
| $\tilde{\Delta}_c L_{eff}$ | 6 | 4 | 2 | 1 |
| Yield displacement (mm) | | | | |
| $\tilde{\Delta}_y^+ L_{eff}$ | 23 | 22 | 17.5 | 15 |
| $\tilde{\Delta}_y^- L_{eff}$ | 23 | 19 | 15 | 10.5 |
| Deteriorate displacement (mm) | | | | |
| $\tilde{\Delta}_d^+ L_{eff}$ | 54.5 | 49 | 34 | 20.5 |
| $\tilde{\Delta}_d^- L_{eff}$ | 54.5 | 47 | 27.5 | 14 |
| Ultimate displacement (mm) | | | | |
| $\tilde{\Delta}_u^+ L_{eff}$ | 87 | 80 | 53 | 32.5 |
| $\tilde{\Delta}_u^- L_{eff}$ | 87 | 72 | 40 | 19.5 |

$$\tilde{\Delta}_c^+ = e^{-0.565r} \Delta_c \tag{11}$$

$$\tilde{\Delta}_c^- = e^{-0.565r} \Delta_c \tag{12}$$

$$\tilde{\Delta}_y^+ = (1 - 0.087r) \Delta_y \tag{13}$$

$$\tilde{\Delta}_y^- = e^{-0.026r} \Delta_y \tag{14}$$

$$\Delta_d^+ = (2.37e^{-0.246r}) \Delta_y \tag{15}$$

$$\Delta_d^- = (2.37e^{-0.34r}) \Delta_y \tag{16}$$

$$\Delta_u^+ = (3.78e^{-0.246r}) \Delta_y \tag{17}$$

$$\tilde{\Delta}_u^- = e^{-0.34r} \Delta_y \tag{18}$$

in which $\Delta_c$ means the crack drift and $\Delta_y$ means the yield drift of column under cyclic bending, respectively.

In order to apply the model, the cracking load $F_c$ and the yield load $F_y$ of the column under cyclic bending have to be evaluated. The cracking load $F_c$ is defined as the load when the principal tensile stress is equal to $0.33\sqrt{f_c'}$ MPa and the yield load $F_y$ can be obtained by the classic theory [12]. The cracking drift $\Delta_c$and yield drift $\Delta_y$are calculated from Eqs. (3) and (4) according to the elastic flexural stiffness $k_{F1}$and degradation flexural stiffness $k_{F2}$. $k_{F1}$ and $k_{F2}$ have the forms as

$$k_{F1} = 3E_c I_{tr} / L_{eff}^3 \tag{19}$$

$$k_{F2} = \alpha(3E_c I_{tr} / L_{eff}^3) \tag{20}$$

where $E_c$ denotes Young's modulus of concrete and $I_{tr}$ denotes the transformed concrete section of column. The coefficient $\alpha$ is taken as 0.167 based on the test results of column under cyclic unilateral loading [17]. Then the flexural primary curve of a column under

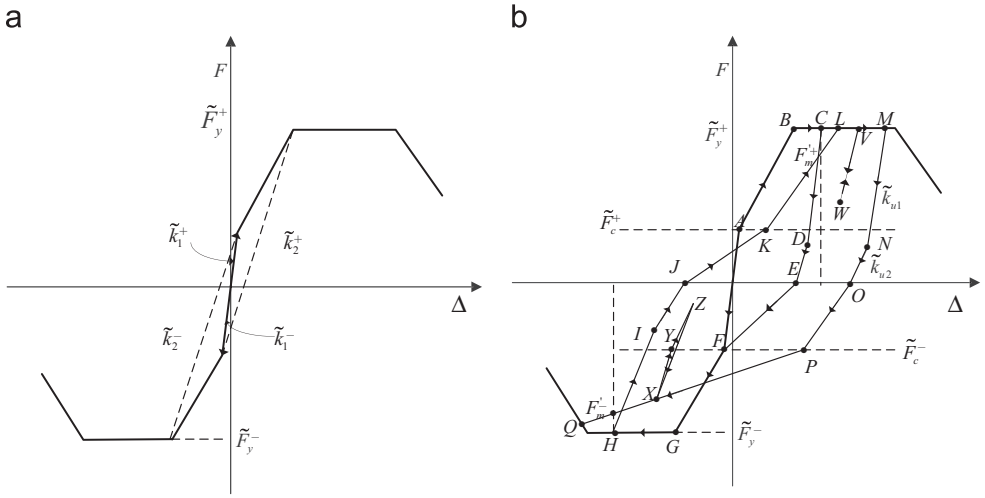


**Fig.21.** Unloading and reloading rules for proposed flexure hysteretic mode; (a) slopes used in defining unloading branches, and (b) sample segments.

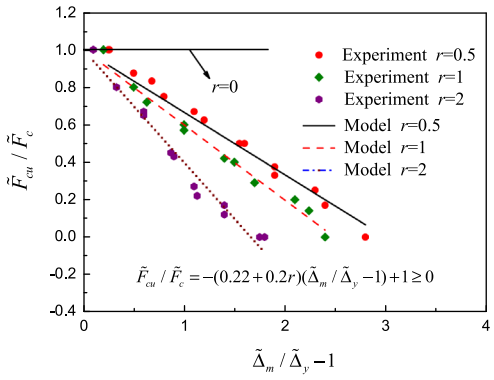


**Fig. 22.** Variation of $\tilde{F}_{cu}/\tilde{F}_c$ with $\tilde{\Delta}_m/\tilde{\Delta}_y - 1$ and $r$.

combined action with a value of rotation-drift ratio $r$ can be evaluated by Eqs. (6)-(18).

### 5.2. Unloading rules

Two slopes of the primary are used as flags to define unloading rules of cyclic loading. As shown in Fig.21 (a), the slope $\tilde{k}_1$ which is equal to $\tilde{k}_{F1}$ is the line connecting the origin to the cracking point in the quadrant unloading taking place, and the slope $\tilde{k}_2$ is the line connecting the yield point in the same quadrant to the cracking point in the opposite direction. It is noted that the parameters of positive loading are represented with $X^+$, while the parameters of negative loading are represented with $X^-$.

Examination of experimental data indicates that unloading follows approximately a straight line from the load reversal point to a point on zero load axis if unloading starts between the cracking load and yield load, and the yield load has not been exceeded in the direction of loading. The slope of this line varies linearly between $\tilde{k}_1$and $\tilde{k}_2$, which is proposed as a function of displacement ductility. If the yield load is exceeded, unloading curve changes slope in a critical load which decreases with the increase of the displacement ductility. It can be seen that the slope of the portion below the critical load is flatter than the portion above. The unloading rules for the proposed model are stated as follows. Fig.21 (b) shows how the column behavior along the flexural hysteretic paths.

1. If the lateral force at the beginning of unloading is less than the cracking load $\tilde{F}_c$ and $\tilde{F}_c$ has not been previously exceeded in either direction, unloading follows the primary curve.
2. If $\tilde{F}_c$ has been exceeded at least once in one direction and the yield load $\tilde{F}_y$ has not been previously exceeded in the quadrant unloading taking place, unloading follow a straight line up to the zero load axis. If unloading from a load is higher than $\tilde{F}_c$, the unloading stiffness is given by Eq. (21). If unloading from a load is lower than $\tilde{F}_c$, the unloading stiffness is equal to $\tilde{k}_1$.

$$\tilde{k} = \tilde{k}_1 - \frac{\tilde{k}_1 - \tilde{k}_2}{\tilde{\Delta}_y - \tilde{\Delta}_c}(\tilde{\Delta}_y - \tilde{\Delta}_c) \tag{21}$$

3. If $\tilde{F}_y$ has been exceeded at least once in the quadrant where the unloading is taking place, unloading stiffness above the critical load $\tilde{F}_{cu}$ is given by Eq.22 (path $C\rightarrow D, H\rightarrow I, M\rightarrow N, V\rightarrow W\ X\rightarrow Y$), and below the critical load$\tilde{F}_{cu}$ is given by Eq.23 (path $D\rightarrow E, I\rightarrow J, N\rightarrow O, Y\rightarrow Z$).$\tilde{F}_{cu}$ may be approximated as Eqs.24 and 25.

$$\tilde{k}_{u1} = \tilde{k}_2 1.4e^{-0.125(\tilde{\Delta}/\tilde{\Delta}_y)^{0.25}}(1-0.016\tilde{\Delta}/\tilde{\Delta}_y)^{3.5} \tag{22}$$

$$\tilde{k}_{u2} = 0.6\tilde{k}_2 1.3e^{-0.125(\tilde{\Delta}/\tilde{\Delta}_y)^{0.35}}(1-0.020\tilde{\Delta}/\tilde{\Delta}_y)^{4.5} \tag{23}$$

$$\frac{\tilde{F}_{cu}}{\tilde{F}_c} = -(0.22+0.2r)(\frac{\tilde{\Delta}_m}{\tilde{\Delta}_y}-1)+1 \geq 0, r>0 \tag{24}$$

$$\tilde{F}_{cu} = \tilde{F}_c, r=0 \tag{25}$$

in which $\tilde{\Delta}$ means the displacement at the unloading starts. Eqs. (24) and (25) give a good correlation with the test result as shown in Fig. 22.

### 5.3. Loading and reloading rules

According to the analysis of experimental results, the rules proposed for loading and reloading are stated as follows. The column behaviors along the flexural hysteretic paths are shown in Fig. 21(b).

1. Initial loading and reloading along the primary curve until the load is reversed at a level higher than the cracking load.
2. If the number has not been loaded beyond the cracking load in one direction, the initial loading in that direction aims at the cracking load even if the member has previously experienced inelastic deformations in the opposite direction (path$E\rightarrow F$).
3. If $\tilde{F}_c$ has been exceeded in the direction of loading; (1) reloading up to $\tilde{F}_c$ will follow a straight passing through point $(\tilde{F}_c, \tilde{\Delta}_r)$

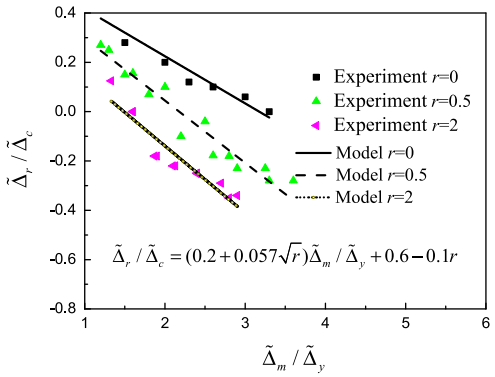


**Fig. 23.** Variation of $\tilde{\Delta}_r/\tilde{\Delta}_c$ with $\tilde{\Delta}_m/\tilde{\Delta}_y$ and $r$.

(path$J\rightarrow K, O\rightarrow P$); (2) reloading beyond $\tilde{F}_c$ will follow a straight line to the primary, passing through point $(\tilde{F}_m{}', \tilde{\Delta}_m)$(path$K\rightarrow L, F\rightarrow G, P\rightarrow Q$); (3) beyond the intersection if reloading branch with the primary curve, loading follows the primary curve (path$L\rightarrow M, G\rightarrow H, P\rightarrow Q$). $\tilde{\Delta}_r$is given by Eq. 26 and $\tilde{F}_m{}'$ is given by Eq. 27.

$$\tilde{\Delta}_r/\tilde{\Delta}_c = (0.2+0.057\sqrt{r})\tilde{\Delta}_m/\tilde{\Delta}_y + 0.6 - 0.1r \tag{26}$$

$$\tilde{F}_m{}' = \tilde{F}_m * e^{[\beta^* n + \gamma^*(\tilde{\Delta}_m/\tilde{\Delta}_y)]} \tag{27}$$

$$\beta = -0.014\sqrt{\tilde{\Delta}_m/\tilde{\Delta}_y} \tag{28}$$

$$\gamma = -0.01\sqrt{n} \tag{29}$$

where $\tilde{\Delta}_m$ denotes the maximum displacement, and Eq. 26 gives a good correlation with the test result as shown in Fig. 23; $\tilde{F}_m$ is the lateral force on primary curve corresponding to the maximum displacement $\tilde{\Delta}_m$, all in the direction of loading. The parameter $n$ is a counter, tracing the successive number of cycles in one direction at the current maximum displacement $\tilde{\Delta}_m$. The value of "$n$" is taken as 1 with the first unloading from the current maximum displacement, which is incremented everytime the load reverses within the maximum displacement range $\tilde{\Delta}_m \pm \tilde{\Delta}_c$. When the current displacement exceeds this range, a new maximum displacement is attained, and $n$ becomes 1 again. Small cycles below the maximum displacement range do not change $n$. It should be noted that the $n$ parameter is assigned two values simultaneously, one for each direction of loading.

4. Reloading in the same quadrant will trace a straight line aiming at the immediately preceding peak point if unloading is completed prior to reaching the zero load axis (path$Z\rightarrow X, W\rightarrow V$).

## 6. Torsional hysteretic model

It can be seen from the experimental results shown in the previous section that the torsional hysteresis shows a high pinching effect. There have been several hysteretic models for flexure, even though some of the available models take account of the pinching phenomenon [12,30], but they cannot be directly used to simulate the torsional hysteresis because none of them was formulated based upon the torsion test data. Tirasit and Kawashima [17] proposed a nonlinear torsional hysteretic model based upon a test of square columns under combined flexural and torsional loadings, but it did not consider the locking and unlocking effect of the spirals. This paper proposes the torsional hysteretic model for the circular columns with spirals, including the factors of rotation-drift ratio $r$ and the number of loading cycles based on the experimental results.

### 6.1. Primary curves

The proposed primary curve for the torsional hysteretic model is developed based upon the experiment as shown in Fig. 24. The column is assumed to be elastic with an initial torsional stiffness $\tilde{k}_{T1}$ until it reaches the torsional strength $\tilde{T}_y$ at the yield rotation $\tilde{\theta}_y$. This torsion remains constant until the column is loaded to $\tilde{\theta}_d$, and then deteriorates with a negative torsional stiffness $\tilde{k}_{T2}$ to the ultimate torsion $\tilde{T}_u$which is equal to 80% of the torsional strength at $\tilde{\theta}_u$. $\tilde{\theta}_u$ is the column rotation at the ultimate torsion. The torsional stiffness $\tilde{k}_{T1}$ and $\tilde{k}_{T2}$ are defined as:

$$\tilde{k}_{T1} = \frac{\tilde{T}_y}{\tilde{\theta}_y} \tag{30}$$

$$\tilde{k}_{T2} = \frac{\tilde{T}_u - \tilde{T}_y}{(\tilde{\theta}_u - \tilde{\theta}_d)} \tag{31}$$

According to the experimental results in the previous section, the behavior of the columns depended on the rotation-drift ratio $r$. Moreover, the torsion of positive loading is generally larger than that of negative loading. The dependency of the torsion and rotation of a column on $r$ is clarified based on the regression analysis. The parameters of positive loading are represented with $X^+$, while the negative loading parameters are represented with $X^-$. Fig. 25 shows that the torsional strength of the column under combined cyclic action $\tilde{T}_y$ increases as $r$ increases, which also approached to the torsional strength of column under cyclic torsion $T_y$ as $r$ increases. This relation may be approximated as

$$\tilde{T}_y^+ = (e^{-0.169/r})T_y^+ \tag{32}$$

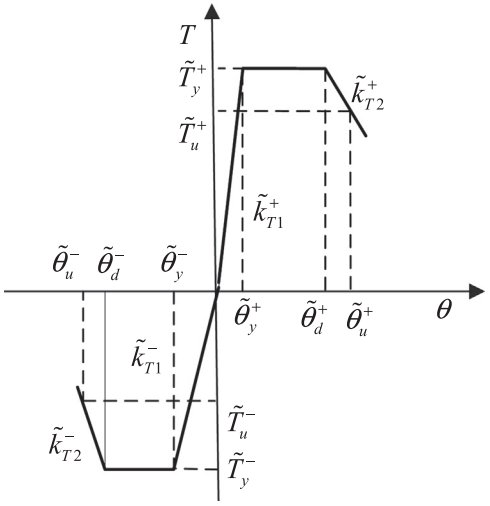


**Fig. 24.** Proposed primary curve for torsion.

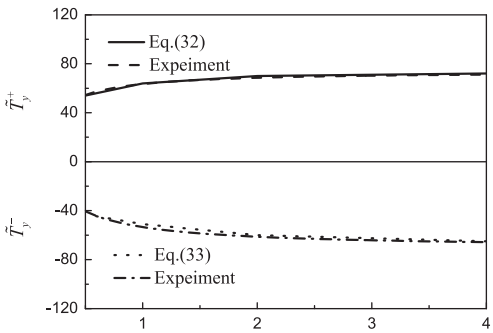


**Fig. 25.** Dependence of the torsional strength on $r$.

$$\tilde{T}_y^- = (e^{-0.277/r})T_y^- \tag{33}$$

$$\tilde{T}_u = 0.8\tilde{T}_y \tag{34}$$

where $T_y$ means the yield torsion of the column under cyclic torsion with axial load. As shown in Fig. 23, the Eqs. (32) and (33) give a good approximation with the lateral experimental results.

Table 5 shows that rotation at yield $\tilde{\theta}_y$, rotation at deteriorates $\tilde{\theta}_d$ and rotation at destroy $\tilde{\theta}_u$ increase as $r$ increases, and converge to the values of the column under cyclic torsion. This relation may be approximated as:

$$\tilde{\theta}_y^+ = (e^{-0.42/r})\theta_y^+ \tag{35}$$

$$\tilde{\theta}_y^- = (e^{-0.49/r})\theta_y^- \tag{36}$$

$$\tilde{\theta}_d^+ = 8(1-e^{-r/1.67})\theta_y^+ \tag{37}$$

$$\tilde{\theta}_d^- = 8(1-e^{-r/2.2})\theta_y^- \tag{38}$$

$$\tilde{\theta}_u^+ = (12e^{-0.84/r})\theta_y^+ \tag{39}$$

$$\tilde{\theta}_u^- = (12e^{-0.9/r})\theta_y^- \tag{40}$$

in which $\theta_y$ is the yield rotation of the column under cyclic torsion with axial load.

In order to use the torsional primary curve, the torsional strength $T_y$ and yield rotation $\theta_y$ of the column under cyclic torsion has to be estimated. $T_y$ may be estimated by the space truss analogy theory [31] and the modified space truss analogy theory [32]. $\theta_y$ can be calculated by Eq.(30) based on the initial torsional stiffness $k_{T1}$. $k_{T1}$ is shown as below:

$$k_{T1} = \gamma(G_c J/L_{eff}) \tag{41}$$

where $G_c$ is the shear modulus of concrete and $J$ is the torsional constant of the column section, and the term in the parenthesis is the gross torsional stiffness of the column. The coefficient $\alpha$ is 0.681 obtained from the experimental results of the columns under cyclic torsion with axial load [12]. Subsequently, the torsional primary curve of a column under combined bending and torsion with a value of $r$ can be further constructed by Eqs. (32)–(40).

**Table 5**
Dependence of $\tilde{\theta}_y$, $\tilde{\theta}_d$and $\tilde{\theta}_u$ on $r$

| $r$ | Yield rotation (rad) | | Deteriorate rotation (rad) | | Ultimate rotation (rad) | |
|---|---|---|---|---|---|---|
| | $\tilde{\theta}_y^+$ | $\tilde{\theta}_y^-$ | $\tilde{\theta}_d^+$ | $\tilde{\theta}_d^-$ | $\tilde{\theta}_u^+$ | $\tilde{\theta}_u^-$ |
| ∞ | 0.0042 | 0.004 | 0.035 | 0.031 | 0.053 | 0.047 |
| 4 | 0.0038 | 0.0035 | 0.033 | 0.026 | 0.045 | 0.039 |
| 2 | 0.003 | 0.0026 | 0.023 | 0.018 | 0.031 | 0.028 |
| 0.5 | 0.002 | 0.002 | 0.011 | 0.01 | 0.015 | 0.013 |

### 6.2. Unloading rules

Unloading slope depends on the torsion and rotation levels attained at the beginning of unloading. The column is unloaded from the envelope at the point of unloading rotation $\tilde{\theta}_m$ and unloading torsion $\tilde{T}_m$.The unloading rules for the proposed model are stated as follows. The definitions of the model parameters and the column how the column behaves along the flexural hysteretic paths are shown in Fig. 26. In addition, the parameters of positive loading are represented with $X^+$, while the parameters of negative loading are represented with $X^-$.

1. Unloading follows the initial stiffness of the envelope if the torsion at the beginning of unloading is less than the yield torsion $\tilde{T}_y$ in either direction (path1→0, 2→0).
2. If the torsion on one side of hysteresis exceeds $\tilde{T}_y$: (1) Unloading down to critical load will follow a straight line with unloading stiffness $\tilde{k}_{Tu1}$ (path 3→4, 8→9, 14→15); (2) Unloading path below $\tilde{T}_{ur}$ will aim towards the zero torsion axis at $\tilde{\theta}_{su}$, which is the reloading rotation of another loading side of column (path 4→5, 9→10, 9→10, 15→16, 15→16). $\tilde{k}_{Tu1}$, $\tilde{T}_{ur}$ and $\tilde{\theta}_{su}$ may be estimated as

$$\tilde{k}_{Tu1} = \tilde{k}_{T1}(1-0.045\tilde{\theta}_m/\tilde{\theta}_y) \tag{42}$$

$$\tilde{T}_{ur}/\tilde{T}_m = -0.025(\tilde{\theta}_m/\tilde{\theta}_y - 1) + 0.672, \tilde{\theta}_m/\tilde{\theta}_y > 1 \tag{43}$$

$$\tilde{\theta}_{su}/\tilde{\theta}_m = (0.02+0.015/r)(\tilde{\theta}_m/\tilde{\theta}_y - 1) + 0.2 \tag{44}$$

in which $\tilde{k}_{T1}$is the line connecting the origin to the yield point as shown in Fig. 26 (a); $\tilde{\theta}_y$ denotes the yield rotation; $\tilde{\theta}_m$ denotes the maximum rotation;$\tilde{T}_m$ denotes the torsion on primary curve corresponding to the maximum rotation; $\tilde{T}_{ur}$ is torsion of changing

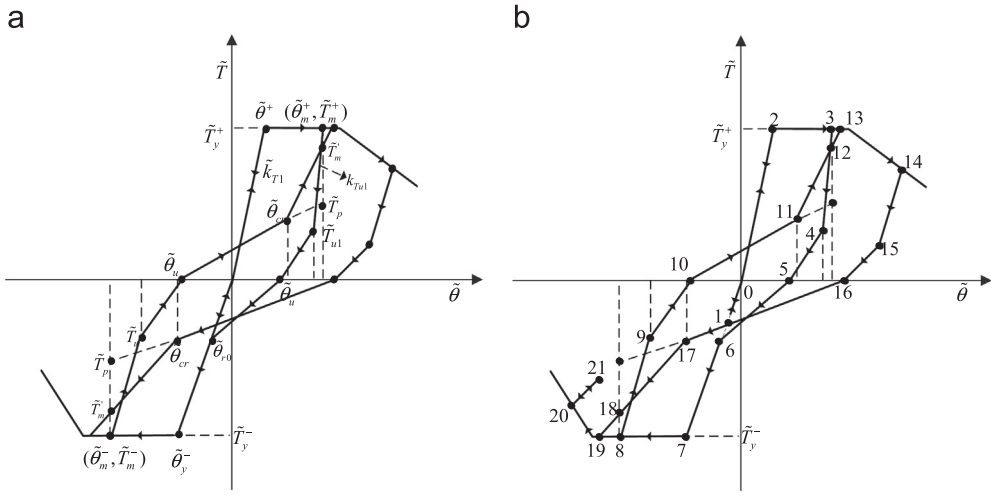


**Fig. 26.** Unloading and reloading rules for proposed torsional hysteretic model; (a) definition of parameters, (b) unloading and reloading rules of proposed model.

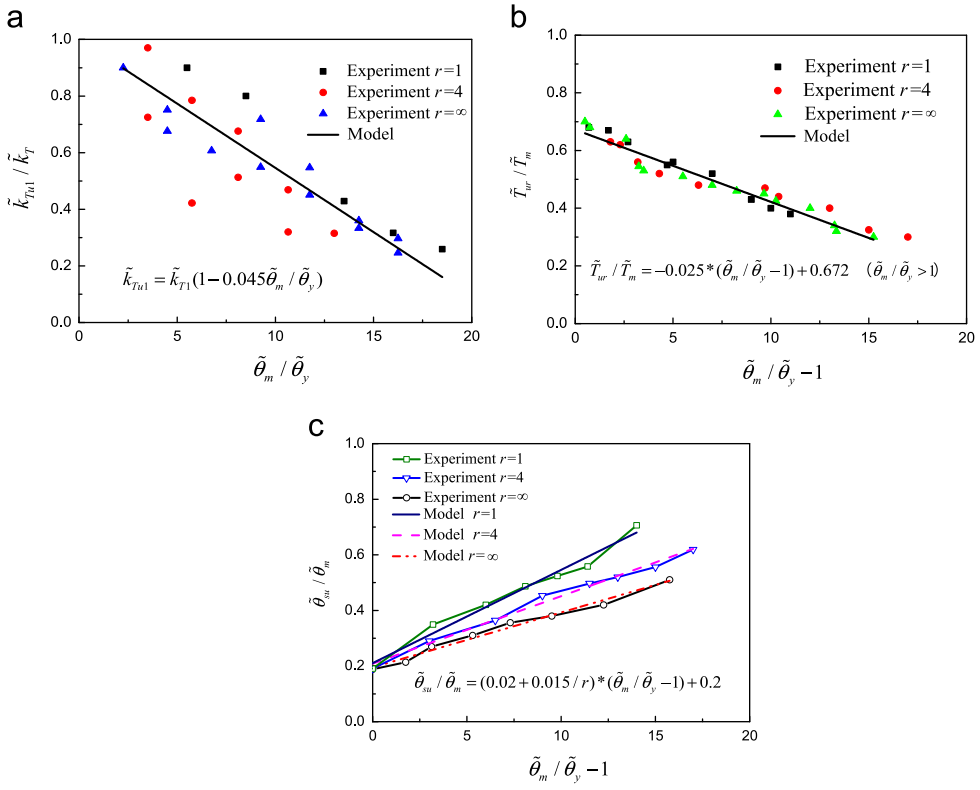


**Fig. 27.** Variations of parameters defining the unloading path; (a) Dependence of $\tilde{k}_{Tu1}/\tilde{k}_T$ on $\tilde{\theta}_m/\tilde{\theta}_y$, (b) Dependence of $\tilde{T}_{ur}/\tilde{T}_m$ on $\tilde{\theta}_m/\tilde{\theta}_y-1$, (c) Dependence of $\tilde{\theta}_{su}/\tilde{\theta}_m$ on $\tilde{\theta}_m/\tilde{\theta}_y-1$.

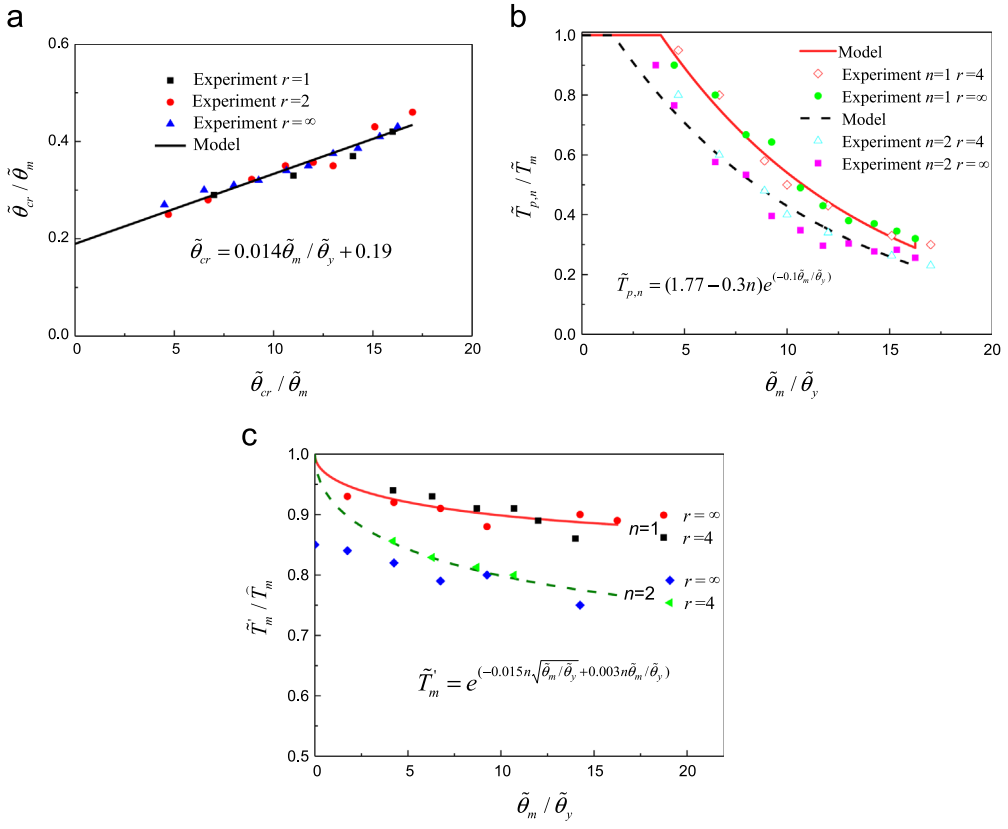


**Fig. 28.** Variations of parameters defining the reloading path; (a) Dependence of $\tilde{\theta}_{cr}/\tilde{\theta}_m$ on $\tilde{\theta}_m/\tilde{\theta}_y$(b) Dependence of $\tilde{T}_{p,n}/\tilde{T}_m$ on $\tilde{\theta}_m/\tilde{\theta}_y$, and (c) Dependence of $\tilde{T}_m'/\tilde{T}_m$ on $\tilde{\theta}_m/\tilde{\theta}_y$.

stiffness due to the reopening of cracks; $\tilde{\theta}_{su}$ is the rotation at the beginning of sliding between crack surfaces. Eqs. (42)–(44) give a good correlation with the test results as shown in Fig. 27.

It is noted that Eq. (42) will appear a zero or negative stiffness when ductility is equal to or greater than 22.2. The problem can be fixed by introducing a new degrading equation, which is given by Eq. (45) [33]. The new equation extends the maximum allowable ductility level to 50 while maintaining the stiffness very close to Eq. (42).

$$\tilde{k}_{Tu1} = \tilde{k}_{T1} 1.4e^{-0.35^{*}(\tilde{\theta}_m/\tilde{\theta}_y)^{0.01}}(1-0.02\tilde{\theta}_m/\tilde{\theta}_y)^{3.5} \quad (45)$$

### 6.3. Loading and reloading rules

According to the analysis of experimental results, the rules proposed for loading and reloading are stated as follows. The definitions of the model parameters and the column how the column behaves along the flexural hysteretic paths are shown in Fig. 26.

1. Initial loading and reloading along the primary curve until the torsion is reversed at a level higher than the yield rotation $\tilde{\theta}_y$ (path $0\rightarrow1, 0\rightarrow2$).
2. If the column hysteresis in the reloading direction has exceeded $\tilde{\theta}_y$; (1) reloading up to $\tilde{\theta}_{cr}$ will follow a straight line passing through point $(\tilde{\theta}_m, \tilde{T}_{p,n})$, which is the point to define the pinching behavior (path $5\rightarrow6, 10\rightarrow11, 16\rightarrow17$); (2) reloading beyond $\tilde{\theta}_{cr}$ will follow a straight line to the primary passing through point $(\tilde{T}_m{}', \tilde{\theta}_m)$, which is used to defined the strength degradation (path $6\rightarrow7, 11\rightarrow13, 17\rightarrow19$); (3) beyond the intersection if reloading the branch with the primary curve, loading follows the primary curve(path $13\rightarrow14, 19\rightarrow20$).$\tilde{T}_{p,n}$ given by Eqs.46 and 47; $\tilde{\theta}_{cr}$ is given by Eq.48; $\tilde{T}_m{}'$ is given by Eq.49.

$$\tilde{T}_{p,n} = (1.77-0.3n)e^{(-0.1\tilde{\theta}_m/\tilde{\theta}_y)} \quad (46)$$

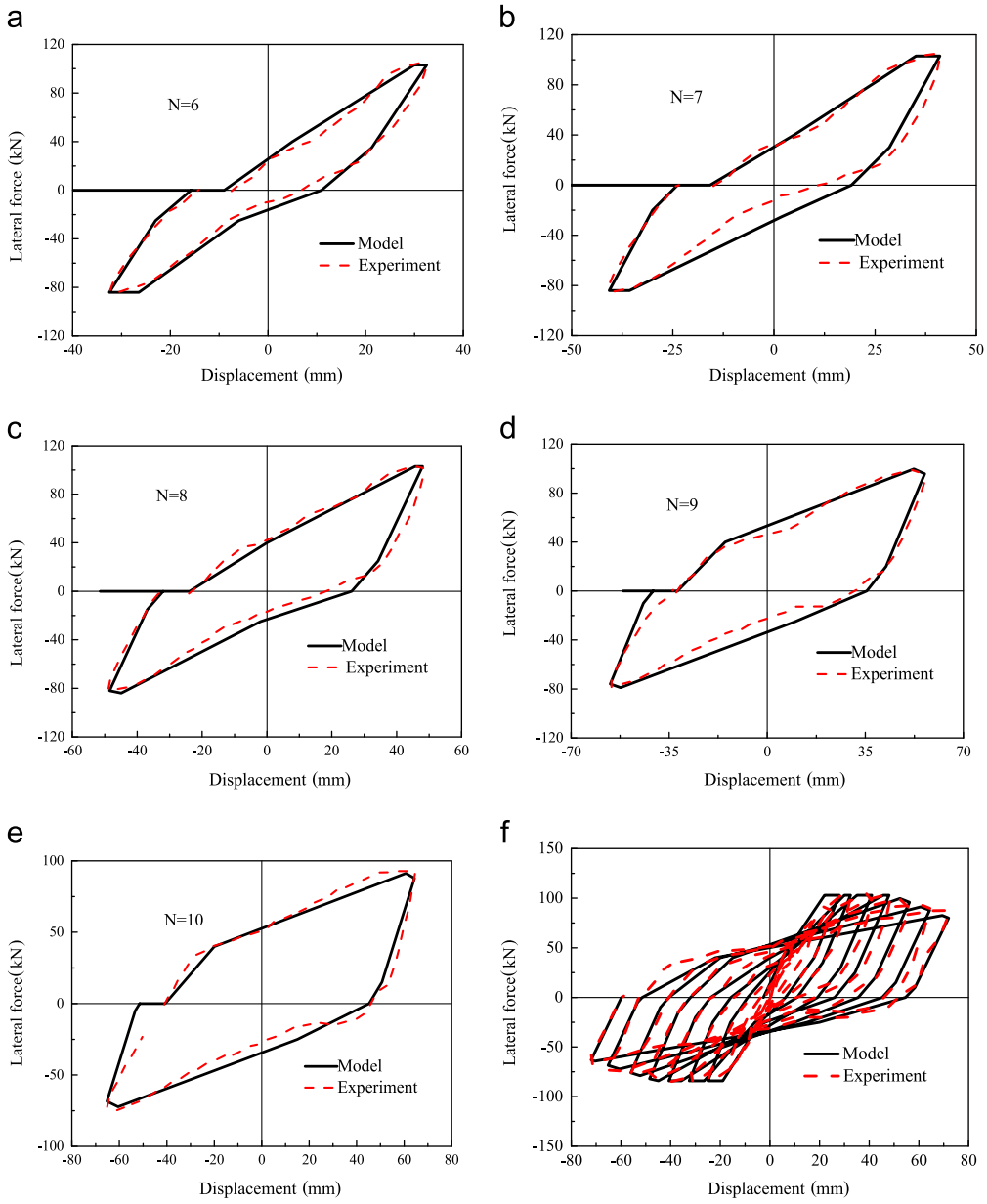


**Fig. 29.** Comparison of the proposed flexural hysteretic model and the experimental result of column S3 ($r$=0.5).

$$\tilde{T}_{p,n} \le \tilde{T}_m \tag{47}$$

$$\tilde{\theta}_{cr} = 0.014\tilde{\theta}_m/\tilde{\theta}_y + 0.19 \tag{48}$$

$$\tilde{T}_m{}' = e^{(-0.015n\sqrt{\tilde{\theta}_m/\tilde{\theta}_y} + 0.003n\tilde{\theta}_m/\tilde{\theta}_y)} \tag{49}$$

It can be seen from Fig. 28 that Eqs. (46)–(49) have a good agreement with the experimental observations. The parameter $n$ is a counter, tracing the successive number of cycles in one direction at the maximum rotation $\tilde{\theta}_m$. The value of "$n$" is taken as 1 when the first unloading from the current maximum rotation, which is incremented everytime the load reverses within the maximum rotation range $(1 \pm 0.05)\tilde{\theta}_m$. When the current rotation exceeds this range, a new maximum rotation is attained, and $n$ becomes 1 again. Small cycles below the maximum rotation range do not change $n$. It should be noted that the parameter $n$ is assigned two values simultaneously, one for each direction of loading.

3. Reloading in the same quadrant will trace a straight line aiming at the immediately preceding peak point if unloading is completed prior to reaching the zero load axis (path20→21).

## 7. Comparison of analytical and experimental hysteresis loops

Fig. 29 compares the results obtained from the proposed flexural hysteretic model with the experimental data of column S3 under combined cyclic action with $r=0.5$. Fig. 30 compares the results obtained from the proposed torsion hysteretic model with the experimental data of column S2 under cyclic torsion. In the experiment, the lateral drift and rotation were simultaneously applied two cycles at every loading step, and the first lap of cyclic loading value is taken to compare with the proposed hysteretic model. Here, N is used to represent the number of loading steps. In addition, Fig. 31 compares the results obtained from the proposed hysteretic model with the experimental data of column

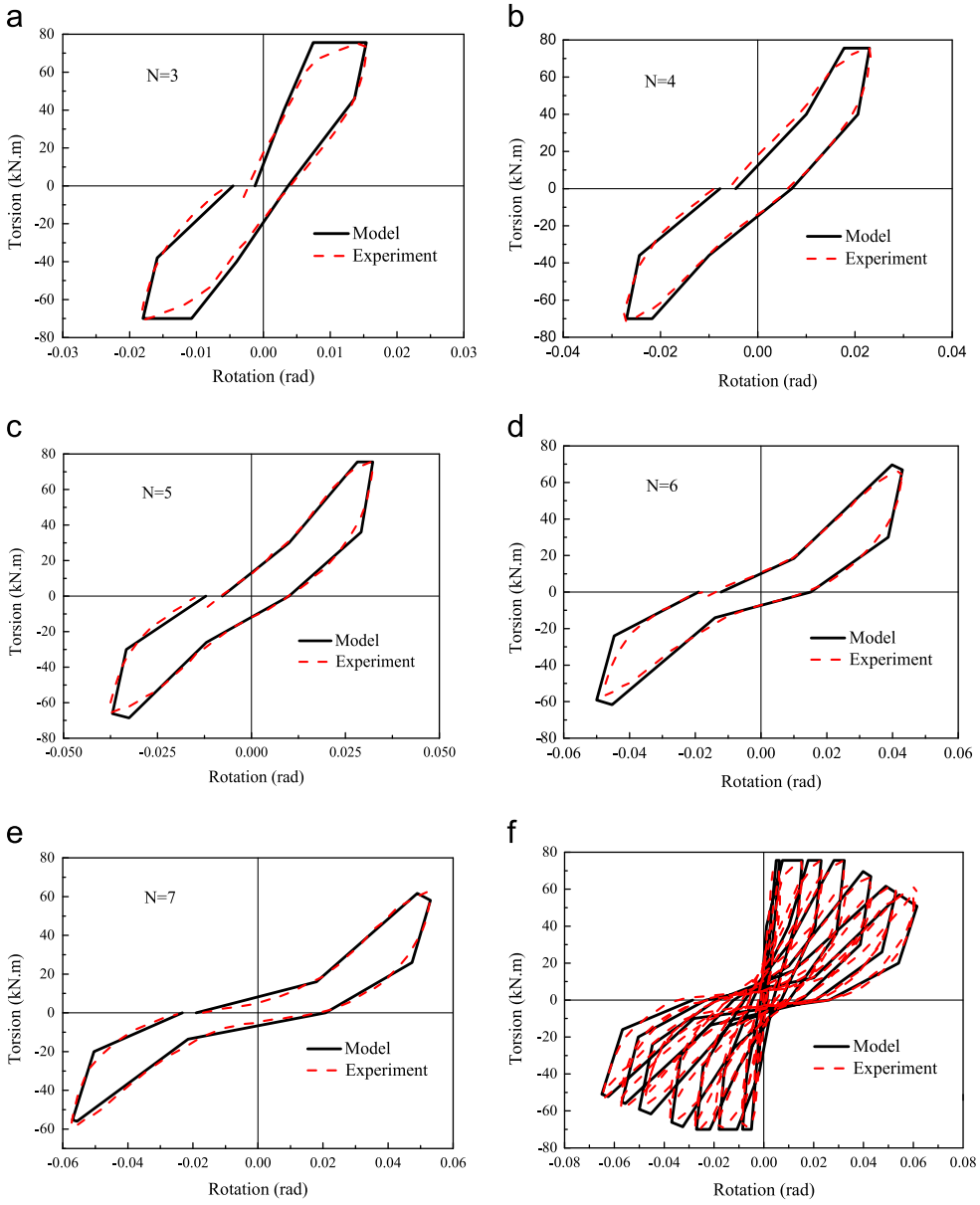


**Fig. 30.** Comparison of the proposed torsional hysteretic model and the experimental result of column S2 ($r=\infty$).

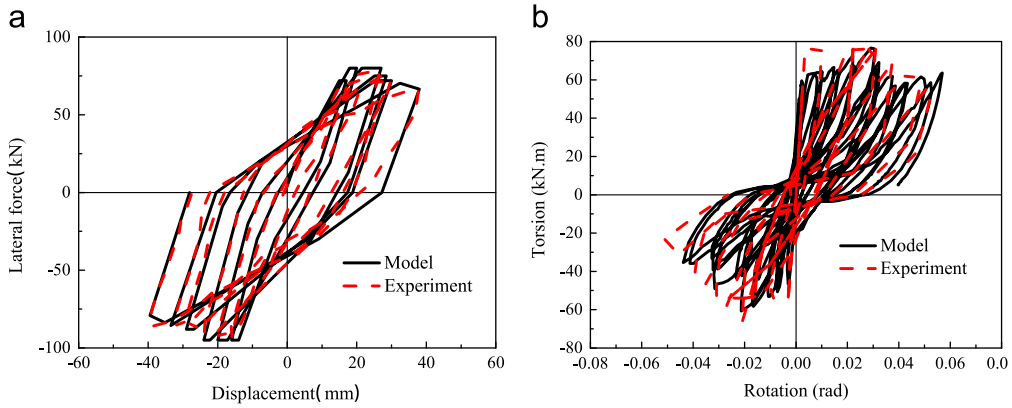


**Fig. 31.** Comparison of the proposed hysteretic model and the experimental result; (a) flexural hysteresis (S4, $r=2$) and (b) torsional hysteresis (S5, $r=4$).

S4 ($r=2$) and S5 ($r=4$). It can be seen that the proposed hysteretic models give a good agreement with the experimental result.

It should be noted that those empirical models are developed for circle columns with a single spiral stirrup and $r$ ranging from 0.5 to 4. Under the condition of meeting the design codes with supplementary stirrups in seismic areas, the additional stirrups could delay the longitudinal reinforcement buckling and enhance the ultimate displacement, and magnitude of axial load has a great influence on the hysteresis characteristics and ultimate deformation of columns [34]. So the proposed model in this paper is limited to RC bridge columns subjected to combined flexural and torsional loadings and the validation of the proposed model outside this range and different tie configurations requires further clarification.

## 8. Conclusions

The test results for twelve circular RC bridge columns under pure bending, pure torsion, and combined loadings were presented and the effects of rotation-drift ratio on strength, stiffness, and damage characteristics was investigated. Furthermore, the influence of aspect ratio, longitudinal reinforcement ratio and type of stirrup on the seismic performance of columns under combined action with the same rotation-drift ratio was discussed. In addition, an empirical flexural hysteretic model and an empirical torsional hysteretic model for circular RC columns with single spiral stirrup under combined cyclic bending and torsion were proposed by clarifying the effect of combined loading based on the test results. The following conclusions can be drawn from results obtained:

1. The flexural plastic hinge was at the base of the column under pure bending, while the torsional plastic hinge near the mid-height of the column under pure torsion. As the rotation-drift ratio increases, the length of the plastic hinge zone of the column under combined cyclic bending and torsion suffers damage above the usual plastic hinge zone under flexural loading, and the locations of peak strains in the longitudinal reinforcement were shifted from the base to the middle of column.
2. The flexural strength and ultimate displacement in flexure decreased as the torsion increases, while the torsional strength and ultimate rotation in torsion decreased as the bending moment increases under combined bending and torsion. Hence, it is necessary to take flexural and torsion interaction into account in the design of columns subjected to combined bending and torsion.
3. The torsional strength and ductility levels of the column under pure torsion were different in the positive and negative loading cycles, which were caused by the locking and unlocking effect of the spirals. Likewise, the locking and unlocking effect of the spirals on torsional and flexural envelopes of columns under combined cyclic bending and torsion was quite obvious.
4. The increasing of the reinforcement ratio can improve the flexural strength but there was little contribution to the torsional strength of columns under combined bending and torsion with the same rotation-drift ratio. The decreasing of stirrup spacing can improve the torsional strength of columns, especially the torsional strength of the positive loading cycles, but the influence on the flexural strength of columns under combined bending and torsion with the same rotation-drift ratio is not obvious. Cross spirals can enhance the strength and ductility characteristics and eliminate the locking and unlocking effect.

A four linear backbone and a three linear backbone were proposed to idealize the flexural envelope and torsional envelope of columns under combined flexure and torsion, respectively. The unloading and reloading rules for torsion moment were developed to complete the torsional hysteretic model. Individual hysteresis loops obtained from the proposed model of various ration-drift ratios are compared with those produced by experimental data, which show a good agreement between the experimental data and the model results. And the proposed model is limited to RC bridge columns under combined flexural and torsional loadings within the range of rotation-drift ratios between 0.5 to 4 and similar tie configurations.

## Acknowledgments

This research is jointly funded by the National Natural Science Foundation of China (Grants no.501178008 and No. 51378033), the National Program on Key Basic Research Project (Grant no.2011CB013600) and the Research Project of Beijing Municipal Commission of Education (Grant KZ201410005011). Their financial supports are gratefully acknowledged.

## References

[1] Han Q, Du XL, Liu JB, Li ZX, Li LY, Zhao JF. The seismic damage of highway bridges during 2008 Wenchuan Earthquake. Earthq Eng Eng Vibr 2009;8(2):263–73.
[2] MJN Priestly, Benzoni G. Seismic performance of circular columns with low longitudinal reinforcement ratios. ACI Struct J 1996;93(4):474–85.
[3] MJN Priestly, Seible F, Calvi GM. Seismic design and retrofit of bridges. New York: John Wiley and Sons, Inc; 1996.

[4] Lehman DE, Calderon, AJ, Moehle JP. Behavior and design of slender columns subjected to lateral loading. In: Proceedings of the 6th U.S. National conference on earthquake engineering. Seattle, Washington, United States; 1998.
[5] Weheb NI, Saidi MS, Sanders DH. Seismic performance of rectangular bridge columns with moderate confinement. ACI Struct J 1999;96(2):248–58.
[6] Yeh YK, Mo YL, Yang CY. Seismic performance of rectangular hollow bridge columns. ASCE J Struct Eng 2002;128(1):60–8.
[7] Pinto AV, Molina J, Tsionis G. Cyclic tests on large-scale models of existing bridge piers with rectangular hollow cross-section. Earthq Eng Struct Dyn 2003;32:1995–2012.
[8] Phan V, Saiidi MS, Aderson J, Ghasemi H. Near-fault ground motion effects on reinforced concrete bridge columns. J Struct Eng 2007;133(7):982–9.
[9] Clough RW, Johnston SB. Effect of stiffness degradation on earthquake ductility requirements. In: Proceedings of the 2nd Japan earthquake engineering symposium, Tokyo, Japan; 1966.
[10] Takeda T, Sozen MA, Nielson NN. Reinforced concrete response to simulated earthquakes. J Struct Div 1970;96(12):2557–73.
[11] Park YJ, Ang HS. Mechanistic seismic damage model for reinforced concrete. J Struct Eng 1985;111(4):722–39.
[12] Ozcebe G, Saatcioglu M. Hysteretic shear model for reinforced concrete members. J Struct Eng 1989;115(1):132–48.
[13] Kowalsky MJ, Priestley MJN. Improved analytical model for shear strength of circular reinforced concrete columns in seismic regions. ACI Struct J 2000;97 (3):388–96.
[14] Otsuka H, Wang Y, Takata T, Yoshimura T. Experimental study on the parameters effecting the hysteresis loop of RC members subjected to pure torsion. J Jpn Soc Civil Eng 2003;739(60):93–104.
[15] Otsuka H, Takeshita E, Yabuki W, Wang Y, Yoshimura T, Tsunomoto M. Study on the seismic performance of reinforced concrete columns subjected to torsional moment, bending moment and axial force. In: Proceedings of the 13th world conference on earthquake engineering, Vancouver, Canada; 2004.
[16] Tirasit P., Kawashima K., Watanabe G. An experimental study on the performance of RC columns subjected to cyclic flexural torsional loading. In: Proceedings of the 2nd international conference on urban earthquake engineering, Tokyo, Japan; 2005.
[17] Tirasit P, Kawashima K. Seismic performance of square reinforced concrete columns under combined cyclic flexural and torsional loadings. J Earthq Eng 2007;11:425–52.
[18] Belarbi A., Prakash S.S., Silva P. Flexure-shear-torsion interaction of RC bridge columns. In: Proceedings of the concrete bridge conference, St. Louis, Missouri, United States; 2008.
[19] Belarbi A., Prakash S.S., You Y.M. Effect of spiral ratio on behavior of reinforced concrete bridge columns under combined loadings including torsion. In: Proceedings of the 4th international conference on advances in structural engineering and mechanics, Jeju, Korea; 2008.
[20] Belarbi A, Prakash SS, You YM. Effect of transverse spiral reinforcement on the seismic flexural–shear–torsional behavior of reinforced concrete circular bridge columns. J Struct Eng Mech 2009;33(2):137–58.
[21] Prakash SS, Belarbi A, You YM. Seismic performance of circular RC columns subjected to axial, bending, and torsion with low and moderate shear. J Eng Struct, 32; 2010; 46–59.
[22] Li Q., Belarbi A., Prakash S.S. Seismic performance of square RC bridge columns under combined loading including torsion with low shear. In: Proceedings of the 12th Biennial international conference on engineering, construction, and operations in challenging environments, Honolulu, Hawaii, United States; 2010.
[23] Mullapudi T, Ayoub A. Analysis of reinforced concrete columns subjected to combined axial, flexure, shear, and torsional loads. Las Vegas, Nevada, United States: ASCE Structures Congress; 2011.
[24] Mullapudi T, Ayoub A. Analysis of reinforced concrete columns subjected to combined axial, flexure, shear, and torsional loads. ASCE J Struct Eng 2013;139 (4):561–73.
[25] Li Q, Belarbi A. Damage assessment of square RC bridge columns subjected to torsion combined with axial compression, flexure, and shear. KSCE J Civil Eng 2013;17(3):530–9.
[26] China Ministry of Transportation. Guideline for seismic design of highway bridges. Beijing: China Communications Press; 2008.
[27] ACI Committee 318. Building code requirements for reinforced concrete and commentary (ACI 318-95). Farmington Hills, MI: American Concrete Institute; 1995.
[28] Mosley WH, Hulse R, Bungey JH. Reinforced concrete design to Euocode 2. 7th ed.. New York: Palgrave Macmillan; 2012.
[29] Hindi R, Al-Qattawi M, Elsharief A. Influence of different confinement patterns on the axial behavior of RC columns. New York, United States: ASCE Structures Congress; 2005.
[30] Kunnath SK, Reinhorn AM, Park YJ. Analytical modeling of inelastic seismic response of RC structures. J Struct Eng 1990;116(4):996–1017.
[31] Rahal KN, Collins MP. Analysis of sections subjected to combined shear and torsion-A theoretical model. ACI Struct J 1995;92(4):459–69.
[32] Mo YL, Yang RY. Response of reinforced prestressed concrete box structures to dynamically applied torsion. J Nucl Eng Des 1996;165:25–41.
[33] Xu SY, Zhang J. Hysteretic shear-flexure interaction model of reinforced concrete columns for seismic response assessment of bridges. Earthq Eng. Struct Dyn 2011;40(3):315–37.
[34] Guo ZX, Lu XL. Experimental study on the hysteretic model of columns with high axial compressive ratio. China Civ Eng J 2004;37(5):32–8.